Urban inland wintertime N_2O_5 and $ClNO_2$ influenced by snow-covered ground, air turbulence, and precipitation

Kathryn D. Kulju[1], Stephen M. McNamara[1], Qianjie Chen[1†], Hannah S. Kenagy[1], Jacinta Edebeli[1,2], Jose D. Fuentes[3], Steven B. Bertman[4], Kerri A. Pratt[1,5*]

[1]Department of Chemistry, University of Michigan, Ann Arbor, MI 48109, USA

[2]Paul Scherrer Institut, 5232 Villigen, Switzerland

[3]Department of Meteorology and Atmospheric Science, Pennsylvania State University, University Park, Pennsylvania 16802, USA

[4]Institute of the Environment and Sustainability, Western Michigan University, Kalamazoo, Michigan 49008, USA

[5]Department of Earth and Environmental Sciences, University of Michigan, Ann Arbor, MI 48109, USA

[†]Current: Department of Civil and Environmental Engineering, The Hong Kong Polytechnic University, Hong Kong SAR, China

Correspondence to: Kerri A. Pratt (prattka@umich.edu)

Abstract. The atmospheric multiphase reaction of dinitrogen pentoxide (N_2O_5) with chloride-containing aerosol particles produces nitryl chloride ($ClNO_2$), which has been observed across the globe. The photolysis of $ClNO_2$ produces chlorine radicals and nitrogen dioxide (NO_2), which alter pollutant fates and air quality. However, the effects of local meteorology on near-surface $ClNO_2$ production are not yet well understood, as most observational and modeling studies focus on periods of clear conditions. During a field campaign in Kalamazoo, Michigan from January-February 2018, N_2O_5 and $ClNO_2$ were measured using chemical ionization mass spectrometry, with simultaneous measurements of atmospheric particulate matter and meteorological parameters. We examine the impacts of atmospheric turbulence, precipitation (snow, rain) and fog, and ground cover (snow-covered and bare ground) on the abundances of $ClNO_2$ and N_2O_5. N_2O_5 mole ratios were lowest during periods of lower turbulence and were not

statistically significantly different between snow-covered and bare ground. In contrast, $ClNO_2$ mole ratios were highest, on average, over snow-covered ground, due to saline snowpack $ClNO_2$ production. Both N_2O_5 and $ClNO_2$ mole ratios were lowest, on average, during rainfall and fog because of scavenging, with N_2O_5 scavenging by fog droplets likely contributing to observed increased particulate nitrate concentrations. These observations, specifically those during active precipitation and with snow-covered ground, highlight important processes, including N_2O_5 and $ClNO_2$ wet scavenging, fog nitrate production, and snowpack $ClNO_2$ production, that govern the variability in observed atmospheric chlorine and nitrogen chemistry and are missed when considering only clear conditions.

1 Introduction

Atmospheric halogen radicals are highly oxidizing agents of tropospheric pollutants (Simpson et al., 2015). Following nighttime formation, the photolysis of nitryl chloride ($ClNO_2$) upon sunrise is a source of chlorine radicals (**R1**) at a time when other oxidants, including the hydroxyl radical (OH), are less abundant (Young et al., 2014), leading to enhanced oxidation of volatile organic compounds (Osthoff et al., 2008). $ClNO_2$ photolysis also releases NO_2 (**R1**), thus recycling nitrogen oxides (NO_x=NO+NO_2) that drive ozone formation (Crutzen, 1979).

$$\mathbf{ClNO_2 + h\nu \rightarrow Cl + NO_2} \quad \text{R1}$$

$ClNO_2$ is formed by the multiphase reaction of dinitrogen pentoxide (N_2O_5) on a chloride-containing surface (**R2**), particularly sea spray aerosol (Finlayson-Pitts and Pitts, 1989; Osthoff et al., 2008).

$$\mathbf{N_2O_{5\,(g)} + Cl^-_{(aq)} \rightarrow ClNO_{2\,(g)} + NO_3^-{}_{(aq)}} \quad \text{R2}$$

In the Northern Hemisphere, surface-level $ClNO_2$ abundance is simulated to be highest during winter; this is thought to be due to greater N_2O_5 abundances, shallower mixed layer heights or even stable boundary layers, lower air temperatures, and higher $ClNO_2$ yields (Sarwar et al., 2014). $ClNO_2$ production has been previously studied in the laboratory following the reaction of N_2O_5 with aqueous aerosols (e.g.

Behnke et al., 1997; Bertram and Thornton, 2009; Roberts et al., 2009; Thornton and Abbatt, 2005) and frozen solutions (Lopez-Hilfiker et al., 2012). A recent modeling study suggests that $ClNO_2$ may be produced from heterogeneous reaction on the snowpack, in addition to aerosols (Wang et al., 2020). In addition to marine and coastal environments, $ClNO_2$ has been measured in inland environments, including Boulder, Colorado, USA (Riedel et al., 2013; Thornton et al., 2010), , Calgary, Alberta, Canada (Mielke et al., 2011), Frankfurt, Germany (Phillips et al., 2012), Ji'nan, Shandong, China (e.g. Wang et al., 2017), and southwest of Baoding, Hebei, China (e.g. Tham et al., 2018); in these inland environments, $ClNO_2$ abundance is typically hundreds of parts per trillion (ppt). Recently, a study in Ann Arbor, Michigan identified road salt aerosol as the dominant aerosol chloride source for $ClNO_2$ production during winter (McNamara et al., 2020). Measurements in Kalamazoo, Michigan also identified the road salt-contaminated snowpack as a $ClNO_2$ source (McNamara et al., 2021). A study in coastal British Columbia, Canada suggested scavenging of $ClNO_2$ by rain and/or fog droplets as a potential loss process (Osthoff et al., 2018). However, the authors pointed out that scavenging of the nitrate radical (NO_3), N_2O_5, and $ClNO_2$ have not been constrained by laboratory investigations (in contrast to other gases like sulfur dioxide (SO_2) and ammonia (NH_3)) and so periods of precipitation were excluded from subsequent calculations of N_2O_5 uptake and $ClNO_2$ yield (Osthoff et al., 2018).

N_2O_5, the precursor to $ClNO_2$, is formed from the reaction of NO_2 with NO_3 (**R3**), which is formed from the reaction of NO_2 with ozone (O_3, **R4**). The formation of N_2O_5 from NO_2 and NO_3 is a temperature-dependent equilibrium, with N_2O_5 production favored at lower temperatures (Asaf et al., 2010; Wagner et al., 2013). At a NO_2 background level of 1 parts per billion (ppb), the ratio of N_2O_5:NO_3 (**R3**) is ~1 at 295 K, but this N_2O_5:NO_3 ratio is ~10 at 278 K (Chang et al., 2011). Loss of N_2O_5 is an important terminal sink for nitrogen oxides (NO_x = NO + NO_2) in the troposphere (Simpson et al., 2015). Long-term data show that direct N_2O_5 loss via hydrolysis, to produce nitric acid (HNO_3, **R5**), is most important during winter, and indirect N_2O_5 loss (removal of NO_3 via reaction with hydrocarbons and NO, **R6**-**R7**) is most important during summer (Allan et al., 1999; Geyer et al., 2001; Heintz et al., 1996).

$$\mathbf{NO_3 + NO_2 + M \rightleftharpoons N_2O_5 + M} \quad \text{R3}$$

$$\mathbf{O_3 + NO_2 \longrightarrow O_2 + NO_3} \quad \text{R4}$$

$$\mathbf{N_2O_5\,(g) + H_2O_{(l)} \longrightarrow HNO_3\,(aq)} \quad \text{R5}$$

$$\mathbf{R - C = C - R' + NO_3 \longrightarrow R - C - C(NO_3) - R'} \quad \text{R6}$$

$$\mathbf{NO + NO_3 \longrightarrow 2\,NO_2} \quad \text{R7}$$

Experimental investigations of the impacts of meteorology on N_2O_5 abundance are primarily limited to observations of uptake by fog in coastal regions (Brown et al., 2016; Osthoff et al., 2006; Sommariva et al., 2009; Wood et al., 2005). In addition to forming HNO_3, hydrolysis of N_2O_5 can produce particle-phase nitrate (NO_3^-) (Brown et al., 2004; Osthoff et al., 2006). Particle-phase nitrate has been observed to increase, then subsequently decrease, during fog episodes, which is hypothesized to be the result of N_2O_5 hydrolysis to form nitrate, followed by wet removal of nitrate from the fog layer (Lillis et al., 1999).

The review by Chang et al. (2011) stated that future observation-based research is need to further investigate how N_2O_5 is affected by meteorological conditions, due to its impacts on $ClNO_2$ and particulate matter abundances, as well as on the oxidative capacity of the atmosphere. Many gaps remain in our understanding of the fates and production of N_2O_5 and $ClNO_2$, especially in inland locations, and how they are influenced by meteorological conditions such as precipitation events, fog, and turbulent mixing. Notably, Stanier et al. (2012) identified the impacts of fog and snow cover as important knowledge gaps in understanding wintertime atmospheric composition, and nitrate formation in particular, in the Midwest United States.

The SNow and Atmospheric Chemistry in Kalamazoo (SNACK) field campaign was conducted during January and February 2018 in Kalamazoo, MI on the campus of Western Michigan University (WMU). In our previous publication from this study, we showed photochemical snowpack HONO production due to snow nitrate photolysis (Chen et al., 2019). Through vertical gradient measurements on select nights of the SNACK field campaign, we showed that N_2O_5 deposits at the same rates over bare and snow-covered ground; whereas, while $ClNO_2$ deposits on bare ground, it can be emitted from the saline snow-covered ground, with snow chamber experiments confirming saline snow $ClNO_2$ production (McNamara et al., 2021). Here, we focus on the observational time series of near-surface $ClNO_2$ and its precursor N_2O_5 and examine the influences of precipitation (rain, snow) and fog, atmospheric turbulence,

ground cover (snow-covered vs bare ground), particulate chloride and nitrate, temperature, and relative humidity (RH) on the night-time abundances of these compounds, measured by chemical ionization mass spectrometry. This study provides new insights into the biases associated with modeling and observations focused on cloudless (clear) conditions, which has been shown to impact predictions of aerosol chemical composition (Christiansen et al., 2020).

2 Methods

The sampling site (42.28°N, 85.61°W) on the campus of WMU in Kalamazoo, MI was located next to a field and was approximately 90 m from a major roadway, as previously described by McNamara et al. (2021). As described below, measurements of trace gases (N_2O_5 and $ClNO_2$), $PM_{2.5}$ (particulate matter with a diameter ≤2.5 μm) inorganic chemical composition, three-dimensional wind speed, and temperature were conducted at the field site from January 20 to February 24, 2018. Daily photographs and field notes were used to determine ground cover and spatial extent of snow cover.

Because N_2O_5 and $ClNO_2$ were present almost exclusively at night, we define "nocturnal"/"nighttime" as the period between 18:00 and 8:00 Eastern Standard Time (EST, Coordinated Universal Time (UTC)-5 h), which was approximately ±30 min from sunrise and sunset during the campaign. At the start of the campaign (January 20) sunrise was at 08:05 local time (eastern standard time, EST), and sunset was at 17:42. At the end of the campaign (February 24) sunrise was at 07:23 EST, and sunset was at 18:27.

2.1 Meteorological measurements

Air temperature and three-dimensional wind speed (u, v, and w) were measured from a height of 1.4 m and at a frequency of 20 Hz using a sonic anemometer (model CSAT3, Campbell Scientific Inc., Logan, UT). The sonic anemometer was not operational from February 20-21 due to complications associated with heavy rainfall. Friction velocity (u^*) was calculated from turbulent covariance of three-dimensional wind speed based on 30 minute averaging, where u', v', and w' are fluctuations about the 30

min mean wind speed in its zonal (u), meridional (v), and vertical (w) components, respectively (E1) (Stull, 1988).

$$u^* = (\overline{u'w'^2} + \overline{v'w'^2})^{\frac{1}{4}} \quad \text{E1}$$

Kinematic heat flux ($w'T'$) was also calculated from sonic anemometer data, where w' and T' are deviations in vertical velocity and temperature from five-minute averages, respectively (Monin and Obukhov, 1954). Kinematic heat flux values were then further averaged to obtain 30 min time resolution quantities. This heat flux value describes the transport of thermal energy by eddies; negative values of w'T' indicate heat transport from the atmosphere to the surface and are associated with a temperature inversion (Stull, 1988).

Weather conditions (rain, snow, and fog) and pressure were recorded at the Kalamazoo−Battle Creek International Airport (KAZO), which was located ~7 km to the southeast; data were retrieved from Weather Underground (https://www.wunderground.com/history/daily/us/mi/kalamazoo/KAZO). Weather conditions were reported with a maximum time resolution of 1 h. This relatively long time resolution limits the use of higher frequency data from other measurements, and therefore, we use 30 min averaged data, with the assumption that the weather condition lasted the entire hour. Weather conditions were classified using reported National Weather Service designations: clear weather conditions include fair, cloudy, mostly cloudy, and partly cloudy; snowfall includes light snow, snow, heavy snow, and wintry mix; fog includes fog and haze; and rainfall refers to light rain, rain, heavy rain, and thunderstorms. Wind speed and temperature data were also obtained from this weather station to supplement the rain case study (February 20-21), during which data from the sonic anemometer were unavailable.

2.2 Chemical ionization mass spectrometry measurements

Measurements of N_2O_5 and $ClNO_2$ were conducted using a chemical ionization mass spectrometer (CIMS, THS Instruments) (Liao et al., 2011). The CIMS instrument uses iodide-water reagent ion clusters, $I(H_2O)^-$, to ionize analyte molecules, which are separated and quantified using a quadrupole mass analyzer. The CIMS was housed in a mobile laboratory trailer at the field site, and sampled ambient air at ~300 L min^{-1} through a specialized inlet. The inlet was designed to prevent wall

losses of reactive species by allowing for the sampled air at the center of the ring to be de-coupled from the inlet walls (laminar flow), thereby avoiding wall surfaces (Huey et al., 2004; Neuman et al., 2002), as in previous campaigns (e.g., McNamara et al., 2019). The inlet consisted of a 30 cm long, 4.6 cm i.d. aluminum pipe attached to a stainless-steel ring torus 1.5 m above ground level. The airflow from this inlet was subsampled at 6.6 L min^{-1} into a 48 cm long, 0.95 cm i.d. FEP Teflon tube and through a custom three-way heated valve (30°C) used to obtain calibration and background measurements. Of this airflow, an ozone monitor (model 205, 2B Technologies, Boulder, CO) sub-sampled 1.7 L min^{-1}, and 0.9 L min^{-1} was sub-sampled into the CIMS ion-molecule reaction region, which was held at a constant pressure of 15.5 Torr. $I(H_2O)^-$ reagent ions (Slusher et al., 2004) were generated by passing iodomethane (CH_3I) in nitrogen (N_2) through a ^{210}Po radioactive ion source. The ion-molecule reaction region was humidified using water vapor from an impinger to prevent changes in ambient RH from altering CIMS sensitivity (Kercher et al., 2009; McNamara et al., 2019).

CIMS background measurements were conducted for 2 min every 15 min by passing the ambient air flow through a scrubber containing glass wool and stainless-steel wool (heated to 120°C) which removed N_2O_5 and $ClNO_2$ with 96.4±0.8% and 89±1% efficiency (mean±95% confidence interval), respectively (McNamara et al., 2021). N_2O_5 was monitored at *m/z* 235 ($IN_2O_5^-$), and $ClNO_2$ was monitored at *m/z* 208 ($I^{35}ClNO_2^-$) and *m/z* 210 ($I^{37}ClNO_2^-$), each with dwell times of 1.5 s. $ClNO_2$ was positively identified using its measured isotopic ratio (**Fig. S1**). The 3σ limits of detection (LOD), corresponding to the 2 min background periods, were 1.3 ppt and 0.4 ppt for N_2O_5 and $ClNO_2$, respectively. We report mole ratios as 30 min averages, for which the 3σ LODs for N_2O_5 and $ClNO_2$ are estimated to be 0.3 ppt and 0.1 ppt for N_2O_5 and $ClNO_2$, respectively, calculated in the same manner as Liao et al. (2011). CIMS measurement uncertainties, which include propagated uncertainties associated with calibrations and fluctuations in the background signal, are estimated as 22%+0.3 ppt and 22%+0.1 ppt for 30 min averaged N_2O_5 and $ClNO_2$ mole ratios, respectively. Calibrations in the field were conducted every 2 h by adding 0.2 L min^{-1} of 12.3±0.2 ppb Cl_2 (in N_2) from a permeation source (VICI Metronics, Inc., Poulsbo, WA) to the ambient airflow. The permeation rate was measured by bubbling the permeation output into a solution of potassium iodide and measuring the oxidation product, triiodide (I_3^-), using UV-visible spectrophotometry at 352 nm (Liao et al., 2011). The instrument responses for N_2O_5 and $ClNO_2$ were

calibrated in the laboratory, with calibration factors relative to the response to Cl_2 obtained, as described in McNamara et al. (2019b).

Cl_2 was monitored as $I(Cl_2)^-$ at *m/z* 197 and 199, each with dwell times of 0.5 s. The LOD for Cl_2 at *m/z* 197 was 2.4 ppt (0.6 ppt for 30 min averaged data). Cl_2 was below its estimated LOD for 30 min averaging for 96% of the nighttime periods (and 91% of daytime periods), and therefore these limited data are not discussed. HNO_3 was also monitored as $I(HNO_3)^-$ at *m/z* 190 with a dwell time of 0.5 s and calibrated offline relative to Cl_2 (McNamara et al., 2020). However, there was a high background signal due to poor scrubbing efficiency (12±1%), resulting in a high LOD of 43 ppt (11 ppt for 30 min averaged data). 40% of the nighttime HNO_3 data during the campaign were below the LOD estimated for 30 min averaging, and therefore these data are not discussed in detail in this work. These upper limits for Cl_2 and HNO_3 mole ratios are important to report, given limited measurements of these compounds in urban, snow-covered environments.

2.3 Ambient ion monitor-ion chromatography (AIM-IC)

$PM_{2.5}$ chloride (Cl^-) and nitrate (NO_3^-) were measured by an ambient ion monitor-ion chromatography instrument (AIM-IC; model 9000D, URG Corp., Chapel Hill, NC), as described in Chen et al. (2019). The AIM-IC and custom outdoor sampling inlet is described in detail by Markovic et al. (2012). Briefly, ambient air was sampled at 3 L min^{-1} through a 2.5 µm cyclone at a height of 1.8 m. A parallel-plate wet denuder (PPWD) supplied with diluted H_2O_2 separated soluble inorganic trace gases. Particles entered a supersaturation chamber (SSC), where hygroscopic growth was initiated prior to an inertial particle separator. The PPWD and SSC were placed outside in an insulated and heated aluminum case to reduce the sampling line length. Trace gas and particle samples were collected every hour using concentrator columns (anion, UTAC-ULP1, ultra-trace anion concentrator ultralow pressure; cation, TCC-ULP1, trace cation concentrator ultralow pressure; Thermo Fisher Scientific, Waltham, MA) for measurements every 2-4 h (3 h after January 24) by an ion chromatograph (ICS-2100; Dionex Inc., Sunnyvale, CA). LiF was used as an internal standard. The 3σ LODs for Cl^- and NO_3^- were 0.004 and 0.05 µg m^{-3}, respectively, for 3 h sampling.

2.4 Aerosol size distribution measurements

Aerosol size distributions were measured using a scanning mobility particle sizer (SMPS, model 3082, TSI, Inc., Shoreview, MN), which measured electrical mobility diameter from 14.1-736.5 nm, and an aerodynamic particle sizer (APS, model 3321, TSI, Inc., Shoreview, MN), which measured aerodynamic diameter from 0.5-20 μm. The air was sampled through a 2.5 μm cyclone (URG Corp., Chapel Hill, NC) from an inlet height of ~3 m. This flow was split from a manifold with a total flow rate of 16.8 L min^{-1} into foam-insulated copper tubing for each instrument; the SMPS and APS sub-sampled at 0.3 L min^{-1} and 4.9 L min^{-1}, respectively.

3 Results and Discussion

The field campaign nights from January 20-February 24 were divided into categories to investigate the impacts of weather events (rain, snowfall, fog), ground cover (snow-covered and bare ground), and atmospheric turbulence on the near-surface (~1.5 m above ground) abundances of N_2O_5 and $ClNO_2$ (**Fig. 1**). Time periods that were below LOD (0.3 ppt and 0.1 ppt for 30 min averaged N_2O_5 and $ClNO_2$, respectively) are included in calculations as $0.5 \times LOD$. Data after 08:00 (approximately ±30 min from sunrise, which was at 08:07 on Jan 20 and 07:25 on Feb 24) are not included such that air entrainment from the residual boundary layer, discussed elsewhere (e.g. Tham et al., 2016), does not influence the results discussed below.

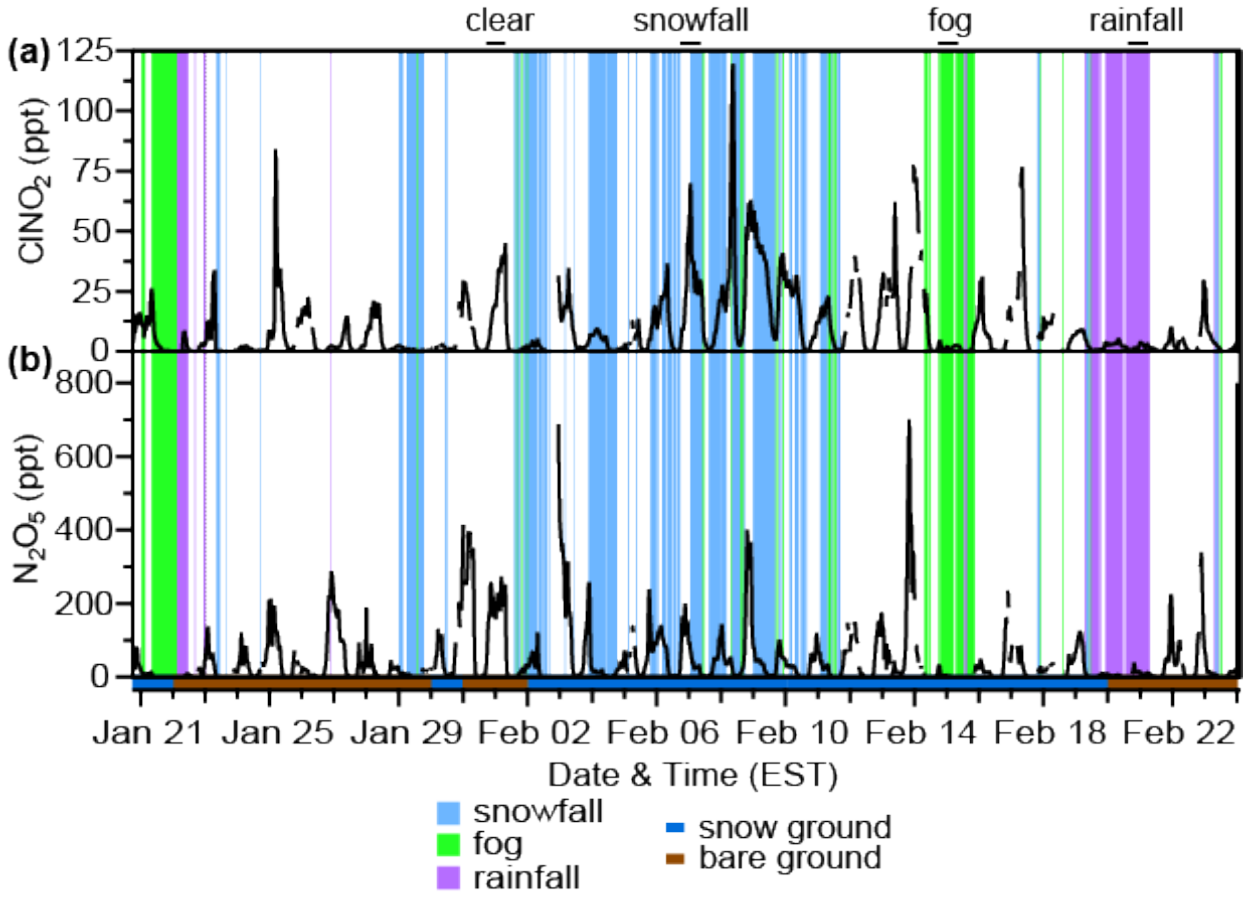

Figure 1: Mole ratios of 30 min averaged **(a)** $ClNO_2$ and **(b)** N_2O_5 during the campaign, and occurrence of snowfall (*light blue*), fog (*green*), and rainfall *(purple)*. The shading below the x-axis represents ground cover – snow *(blue)* or bare ground *(brown)*. The black bars on the top of the plot show the selected case study nights for each weather event type. Between 18:00 and 08:00 h EST, where n=number of 30 min periods, the air was clear 72% of the time [n=726; 363 h], snowfall occurred 16% of the time [n=157; 78.5 h], rainfall occurred 6% of the time [n=63; 31.5 h], and fog occurred 6% of the time [n=58; 29 h]. The ground was snow-covered 57% of the study [20 d] and was bare for 43% of the study [15 d]. Figure S3 gives further details about the occurrence of weather events (rainfall, fog, snowfall) in relation to friction velocity and ground cover.

3.1 Effects of rain, snow, and fog (campaign-wide)

The nighttime abundances of N_2O_5 and $ClNO_2$ during rain, snowfall, and fog were all significantly different ($p<0.05$, six t-tests) from clear conditions (**Fig. 2**). Campaign-wide average nighttime (18:00-08:00) N_2O_5 and $ClNO_2$ mole ratios during clear conditions and each type of weather event are listed in

Table 1, with additional data ($PM_{2.5}$ Cl^- and NO_3^-, temperature, relative humidity, and friction velocity) for these time periods provided in Table S1. Here we discuss observations during these weather events across the entire campaign; example case studies are discussed in Section 3.2. The average nighttime N_2O_5 mole ratios (±95% confidence interval) were 84±5 ppt, 47±2 ppt, 14±2 ppt, and 7.1±0.6 ppt during clear, snowfall, rain, and fog conditions, respectively (**Fig. 2**). In comparison to clear conditions, average N_2O_5 mole ratios were 37±5 ppt (1.8 times), 70±5 ppt (6.0 times), and 77±5 ppt (12 times) lower during snowfall, rain, and fog, respectively. The decrease in N_2O_5 abundance during fog suggests N_2O_5 uptake by fog droplets, and is consistent with previous observations (Brown et al., 2016; Osthoff et al., 2006; Sommariva et al., 2009; Wood et al., 2005). More recently, a study by Osthoff et al. (2018) noted decreased $ClNO_2$ abundance during drizzle/rain and fog during Jul.-Aug. in coastal British Columbia. However, clear conditions are generally the focus of previous N_2O_5 and $ClNO_2$ studies (Chang et al., 2011; Simpson et al., 2015).

Table 1: Mean (±95% confidence interval) mole ratios of N_2O_5 and $ClNO_2$, $PM_{2.5}$ Cl^- and NO_3^- concentrations, temperatures, and relative humidity during each type of weather event (clear, snow, fog, and rain) and ground cover (bare and snow-covered ground) measured across the entire campaign, between 18:00-08:00 EST. The numbers of 30 min periods (n) and percentages of nighttime periods classified as each weather condition are included in parenthesis. Note that bare and snow-covered ground co-existed with the weather conditions, as discussed in Section 3.4. 95% confidence intervals are reported to describe the variabilities in 30 min averaged values of the parameters for the various weather and ground cover conditions.

Weather or Ground Cover Condition	**N_2O_5 (ppt)**	**$ClNO_2$ (ppt)**	**$[Cl^-]$ ($\mu g\ m^{-3}$)**	**$[NO_3^-]$ ($\mu g\ m^{-3}$)**	**Temperature (K)**	**Relative Humidity (%)**
Clear (n=726, 72%)	84±5	11.8±0.7	0.257±0.007	0.95±0.04	270.8±0.3	75.0±0.5
Snowfall (n=157, 16%)	47±2	16.8±0.7	0.258±0.006	0.81±0.03	265.8±0.2	83.0±0.3
Fog (n=58, 6%)	7.1±0.6	5.0±0.6	0.456±0.008	1.38±0.04	276.7±0.2	93.7±0.3
Rain (n=63, 6%)	14±2	2.27±0.06	0.22±0.01	0.126±0.007	282.1±0.2	90.2±0.4

Snow-covered ground (20 d, 57%)	70±5	14.9±0.8	0.30±0.01	1.03±0.04	268.4±0.3	80.0±0.5
Bare ground (15 d, 43%)	68±4	7.0±0.5	0.21±0.01	0.67±0.03	274.8±0.3	75.8±0.6

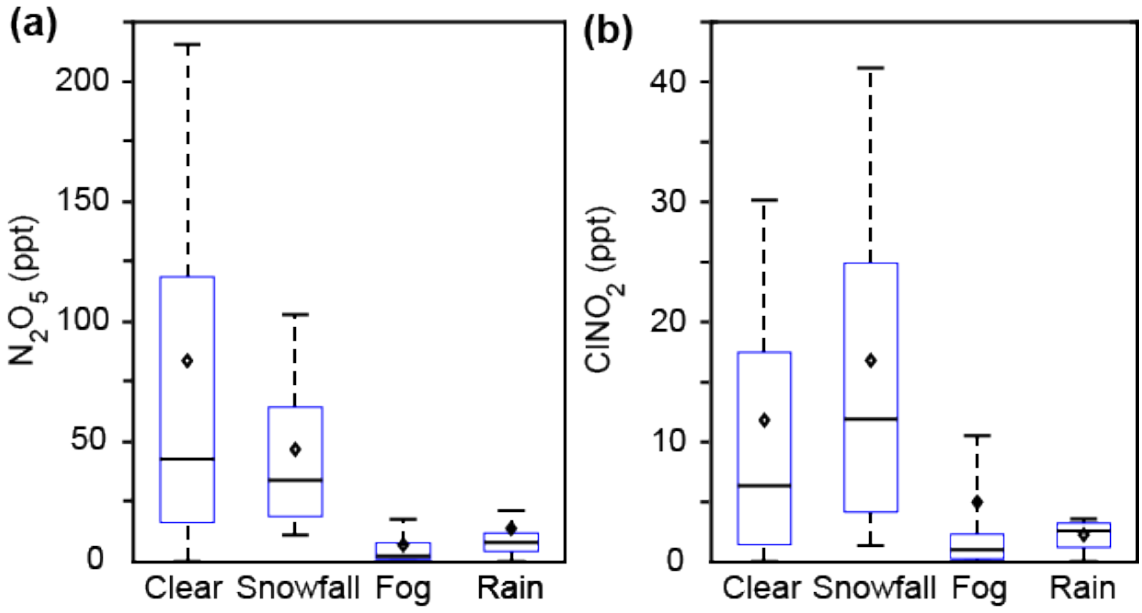

Figure 2: Box plots showing 30 min averaged mole ratios of (a) N_2O_5 and (b) $ClNO_2$ during clear conditions and weather events (snowfall, fog, and rain) from the entire campaign, January 20 - February 24. Bars represent the 10th, 50th, and 90th percentiles, boxes represent the 25th and 75th percentiles, and diamonds represent the means. Only nighttime data between 18:00 and 08:00 EST are included. Data during all weather events (snowfall, fog, rain) are significantly different ($p<0.05$, t-test) from clear conditions.

The average $ClNO_2$ mole ratios were 16.8±0.7 ppt during snowfall, 11.8±0.7 ppt in clear conditions, 5.0±0.6 ppt during fog, and 2.27±0.06 ppt when raining (Fig. 2). In comparison to clear conditions, average $ClNO_2$ mole ratios were 6.8±0.9 ppt (2.4 times) and 9.5±0.7 ppt (5.2 times) lower during fog and rain, respectively. Lower average abundances of $ClNO_2$ during fog and rainfall, compared to clear conditions, are consistent with previous observations (Osthoff et al., 2018) and were likely due

to scavenging either of $ClNO_2$ directly or its precursors (R2). In contrast, average $ClNO_2$ mole ratios were 5±1 ppt (1.4 times) higher during snowfall than clear conditions. This result is surprising, considering that its precursor, N_2O_5, showed lower mole ratios, on average, during snowfall in comparison to clear conditions. We hypothesize that snowpack $ClNO_2$ production contributes to this observation, which is discussed in *Sect. 3.3-3.4*. Particle-phase chloride and nitrate concentrations were not statistically significantly different between clear and snowfall conditions (p=0.96 and 0.08, respectively), nor were aerosol number or surface area concentrations (p=0.06 and 0.31, respectively), as discussed in *Sect. 3.5*. The effects of temperature and relative humidity are discussed in *Sect. 3.5*.

3.2 Effects of rain, snow, and fog (case study nights)

To further examine the behavior of N_2O_5 and $ClNO_2$ mole ratios in response to snowfall, rain, and fog, we present four nocturnal case study periods that were representative of the four different weather conditions (clear, snowfall, fog, and rain) observed during the campaign (**Fig. 3**). Case study nights were chosen to capture a sustained weather event (e.g. >7 h of clear conditions, snowfall, fog, or rainfall). Additionally, ground cover and friction velocity were matched as closely as possible for case study nights to the campaign-wide averages during different types of weather events. Additional data specific to the case studies is provided in the supplemental material (**Table S2**, **Fig. S4-S6**). The clear case night of Jan 31-Feb 01 had no precipitation or fog, an average u* of 0.16±0.01 m s^{-1} (campaign average u* was 0.150±0.004 m s^{-1} during nighttime clear conditions), and bare ground. N_2O_5 mole ratios were fairly stable around 200 ppt (average 200±16 ppt, range 75-274 ppt) throughout the night, with $ClNO_2$ mole ratios increasing steadily between 18:00-07:30 from 1.5 ppt to 45 ppt (average 23±5 ppt, range 0.6-4.5 ppt) (**Fig. 3a**).

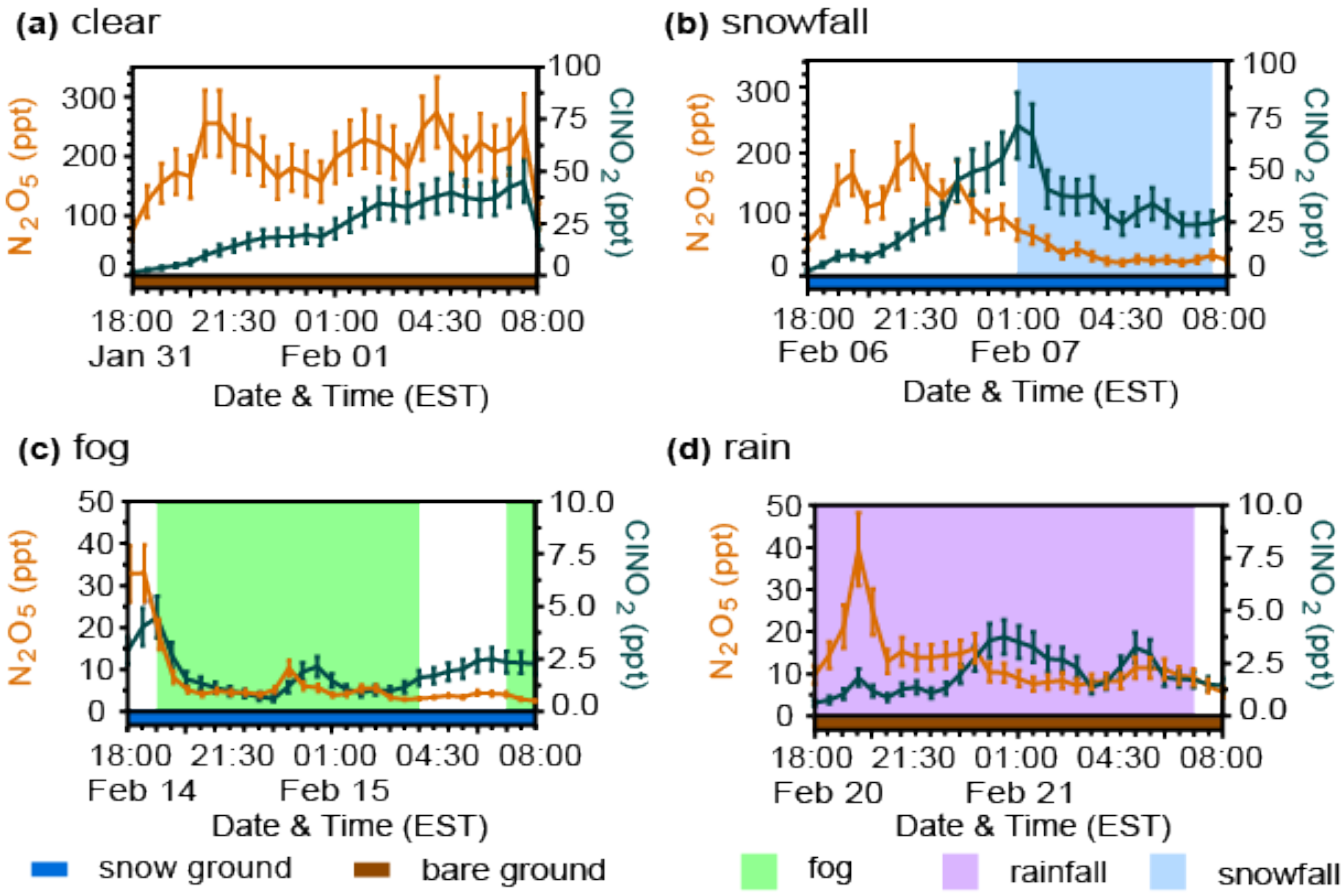

Figure 3: Four example case study periods are shown, corresponding to (a) clear conditions, (b) snowfall, (c) fog, and (d) rainfall. The 30-min averaged abundances of N_2O_5 *(orange)* and $ClNO_2$ *(dark blue)* are displayed for each case. Error bars represent propagated uncertainties. The shading below the x-axis represents ground cover – snow *(blue)* or bare ground *(brown)*.

To discuss changes in gas-phase concentrations during precipitation and fog, we apply the concept of solution equilibrium to the surface layer of a drop (i.e. a rain or fog droplet) in terms of a local equilibrium between the analyte in the gas-phase and the analyte dissolved in the surface layer (Pruppacher and Klett, 1997). This equilibrium can then be described using Henry's law and Henry's law constants (K_H). For N_2O_5, fast, irreversible hydrolysis is assumed, equivalent to an infinite effective K_H (Jacob, 1986; Sander, 2015). For $ClNO_2$, the $K_H = 4.5 \times 10^{-4}$ mol m^{-3} Pa^{-1} at standard temperature (Frenzel et al., 1998; Sander, 2015), showing little variation between ~278 and 294 K. Converting the K_H for $ClNO_2$ to its dimensionless Henry solubility (also called the air-water partitioning coefficient, K_{AW}), as

in Sander (2015), gives a unitless ratio between the aqueous and gas phases of >1 at temperatures above freezing. This means, at equilibrium, $ClNO_2$ is expected to be more abundant in the aqueous-phase than in the gas-phase. The fast irreversible hydrolysis assumed for N_2O_5 makes it more water soluble than $ClNO_2$; therefore, scavenging by liquid droplets is expected for both gas-phase N_2O_5 and $ClNO_2$, but to a greater extent for N_2O_5. Here, we examine the fog and rainfall case studies to characterize the effects of scavenging by aqueous droplets on N_2O_5 and $ClNO_2$ abundance. Variations in N_2O_5 and $ClNO_2$ over the course of the nights are likely due to variability in fog/rainfall that were not resolved by the time resolution of the reported weather conditions, which also do not reflect precipitation rates or fog concentrations that would be expected to vary through the nights.For the fog case night of Feb 14-15, fog was present from 19:00-04:00 and 07:00-08:00 (**Fig. 3c**). This case had an average u* of 0.18±0.02 m s^{-1} (campaign average u* was 0.162±0.007 m s^{-1} during nighttime fog) and snow-covered ground. N_2O_5 mole ratios decreased rapidly from the maximum of 32 ppt at 18:00 and fell to a local minimum of 2.3 ppt at 22:30; it then remained low in abundance (<10 ppt) for the rest of the night, reaching its true minimum of 1.1 ppt at 03:30. $ClNO_2$ mole ratios reached the maximum of 4.5 ppt at 19:00 and then decreased coincident with the appearance of fog and remained low in abundance (<3 ppt) for the rest of the night, reaching its minimum of 0.6 ppt at 23:00. Considering the first hour after the fog onset (19:00-20:00), N_2O_5 mole ratios decreased from 16.6 ppt to 3.4 ppt (decrease of 13.2 ppt or 80%) and $ClNO_2$ mole ratios decreased from 4.5 ppt to 1.6 ppt (decrease of 2.9 ppt or 64%).

Similarly, the rainfall case night of Feb 20-21 was characterized by rainfall from 18:00-07:00 and bare ground (**Fig. 3d**). While sonic anemometer data were unavailable on this night, elevated wind speeds of 2.2-8.9 m s^{-1} (average=5.0±0.5 m s^{-1}) (**Fig. S4** and **Table S2**) are consistent with increased turbulence, with u* likely greater than 0.25 m s^{-1} for the duration of the night (**Fig. S5**). N_2O_5 mole ratios decreased rapidly from the maximum of 40 ppt at 19:30, stabilized at ~15 ppt from 20:30-00:00, and then decreased again to ~10 ppt until 08:00. $ClNO_2$ mole ratios reached the maximum of 3.7 ppt at 00:30, with a second local maximum of 3.0 ppt at 05:30; $ClNO_2$ abundance was <2 ppt before 23:30 and after 06:00. The observations during the fog and rainfall case studies reinforce the trends observed for the campaign averages (**Fig. 2-3**) and illustrate the importance of scavenging by liquid droplets.

The snowfall case night of Feb 06-07 was characterized by snowfall from 01:00-07:30 (**Fig. 3b**), an average u* of 0.06±0.01 m s^{-1} (campaign average u* was 0.129±0.004 m s^{-1} during nighttime snowfall), and snow-covered ground. N_2O_5 mole ratios reached the maximum of 201 ppt at 21:30 and then gradually decreased throughout the rest of the night; it reached its minimum of 22 ppt at 04:00 and then remained low in abundance (22-34 ppt). $ClNO_2$ mole ratios reached the maximum of 70 ppt at 01:00, the same time that snowfall began, and then decreased steadily to the minimum of 24 ppt at 04:30, after which it also remained low in abundance (24-34 ppt). Considering the first hour after snowfall onset (01:00-02:00), N_2O_5 mole ratios decreased from 74.8 ppt to 53.6 ppt (decrease of 21.2 ppt or 28%) and $ClNO_2$ mole ratios decreased from 69.8 ppt to 40.3 ppt (decrease of 29.5 ppt or 42%).

The observations during the snowfall case are also consistent with campaign-wide observations (**Fig. 2-3**). In comparison to the clear case, the snowfall case night shows that N_2O_5 mole ratios were generally lower during snowfall (by 2.1 times, on average), whereas $ClNO_2$ mole ratios were typically higher during snowfall (by 1.4 times, on average). Even though the clear case study had the highest mole ratios of N_2O_5, the snowfall case study had the highest mole ratios of $ClNO_2$ (**Fig. 3** and **Table S2**). The clear and snowfall case studies differed in both ground cover and air turbulence, with lower friction velocity (average=0.06±0.01 m s^{-1}) and snow-covered ground observed during the snowfall case and intermediate friction velocity (average=0.16±0.01 m s^{-1}) and bare ground observed during the clear case study. Additional effects on the abundances of N_2O_5 and $ClNO_2$ are further investigated in the following sections.

3.3 Effects of turbulence

Turbulent mixing (quantified here using friction velocity, u*, **E1**) affects abundances of surface-level trace gases (Stull, 1988). Stronger turbulent mixing promotes vertical transport, and weaker turbulent mixing keeps trace gases near the ground (Stull, 1988). Turbulence regimes were divided within the context of our study to allow subsequent analysis by binning with sufficient data in each bin. Here, lower turbulence refers to u* < 0.1 m s^{-1}, higher turbulence is u* > 0.25 m s^{-1}, and mid-turbulence refers to 0.1 < u* < 0.25 m s^{-1}. Lower turbulence occurred 39% of the time, mid-turbulence occurred 42% of the time, and higher turbulence occurred 14% of the time (**Fig. S3**). For context, typical u* values range

from near 0 m s^{-1} during calm conditions to 1 m s^{-1} during strong winds; moderate wind values often have u* values near 0.5 m s^{-1} (Stull, 2017). Lower friction velocity, in general, was observed during our study, which focuses on nighttime measurements during winter. We investigate the effects of atmospheric turbulence on the abundances of $ClNO_2$ and N_2O_5 by comparing lower (u* < 0.1 m s^{-1}) and higher turbulence (u* > 0.25 m s^{-1}) periods across 30 min averaged periods for a full diel cycle during the entire campaign (**Fig. 4**). Periods of snowfall, fog, and rainfall were included in this analysis due to the relationships which exist between weather events and friction velocity; for example, snowfall occurred most often during lower turbulence conditions, while rainfall occurred most often during higher turbulence conditions, the effects of which are further discussed in *Sect. 3.5*.

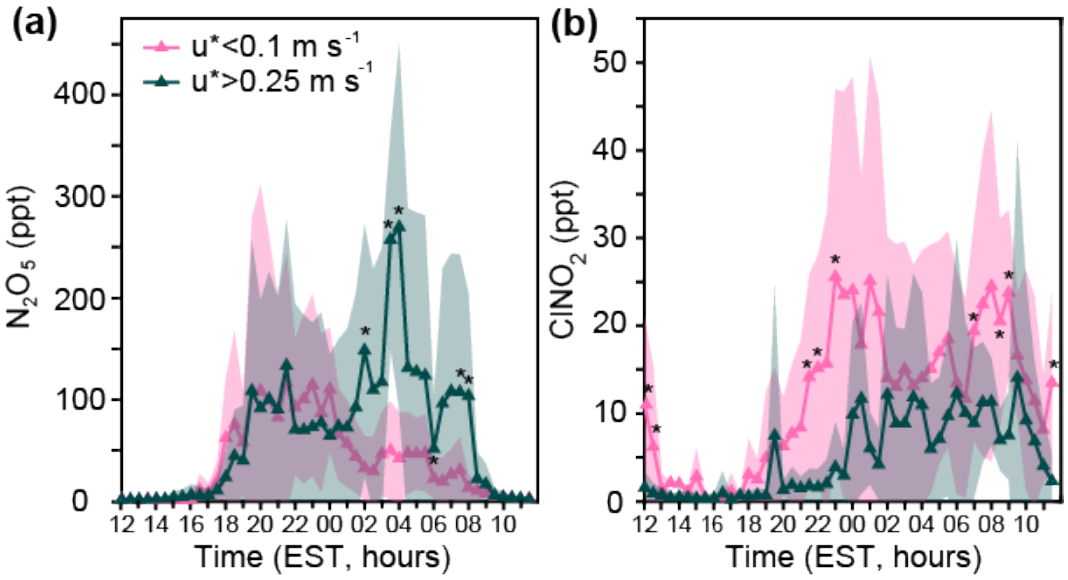

Figure 4. Campaign-wide diel patterns of 30 min averaged (a) N_2O_5 and (b) $ClNO_2$, binned by lower (u*<0.1 m s^{-1}) and higher (u*>0.25 m s^{-1}) friction velocities. Shading represents one standard deviation. Asterisks represent statistically significant (t-test) differences at the p<0.05 level between the lower and higher friction velocity bins for each 30 min period from January 20-February 24 (excluding February 20-21 when the sonic anemometer was not operational). The number of 30 min time periods, from 18:00-08:00, is reported as n. Lower turbulence occurred 39% of the time (n=391) and higher turbulence occurred 14% (n=137) of the time; sonic anemometer data were unavailable for 5% (n=53) of nighttime periods.

Significantly higher (p<0.05, t-test) N_2O_5 mole ratios were observed under higher turbulence conditions at 02:00, 03:30, 04:00, 06:00, and 07:30, and 08:00 (**Fig. 4a**). These statistically significant

time points correspond to, on average, 5.9 times higher N_2O_5 mole ratios during higher turbulence conditions, in comparison to lower turbulence conditions. Considering the entire period of 02:00-08:00, N_2O_5 mole ratios were 4.0 times higher, on average, during higher turbulence conditions in comparison to lower turbulence conditions. Before 02:00, no statistically significant differences were observed in N_2O_5 abundance between higher and lower turbulence conditions, suggesting that titration of NO_3 (N_2O_5 precursor, R3) by NO was not significant during these time periods. Considering the nighttime period as a whole (18:00-08:00), N_2O_5 mole ratios were higher by 24±4ppt (1.6-fold) during higher turbulence, in comparison to lower turbulence conditions. For context in relation to the various weather conditions, higher turbulence ($u^*>0.25$ m s^{-1}) was present for 13%, 9%, 19%, and 17% of the time during clear, snowfall, fog, and rainfall conditions, respectively (**Fig. S3**).

NO_3, a reactant necessary to produce N_2O_5 (**R3**), is sensitive to changes in NO and O_3 levels; in particular, titration of NO_3 by NO (**R7**) is an important loss process at night and results in lower N_2O_5 production (Asaf et al., 2010). Therefore, when NO is emitted and confined near the ground in the stable nocturnal boundary layer, NO_3 has a short near-surface lifetime, thereby limiting N_2O_5 levels (Brown et al., 2007; Wang et al., 2006). Such stable conditions are associated with nocturnal temperature inversions, which can be observed during wintertime in the mid-latitudes (Leblanc and Hauchecorne, 1997). As expressed by kinematic heat flux less than 0 K m s^{-1}, a nocturnal temperature inversion was observed every night of the study (**Fig. S7**). As expected during more stable conditions, reduced N_2O_5 mole ratios were observed during nighttime lower turbulence ($u^*<0.1$ m s^{-1}) compared to higher turbulence ($u^*>0.25$ m s^{-1}) periods (average N_2O_5 mole ratios of 40±2 ppt and 64±3 ppt, respectively).

Vehicle NO_x emissions from the nearby roadway location ~80 m away (McNamara et al., 2021) are suggested to control the magnitude of the nighttime titration effect at the field site, as few time periods overnight were statistically different in O_3 mole ratios between the lower and higher turbulence conditions, on average (**Fig. S8**). However, despite 39% of the nighttime periods being characterized by lower turbulence ($u^*<0.1$ m s^{-1}) (**Fig. S3**), N_2O_5 mole ratios during the full campaign ranged from 0.15-702 ppt (mean 44±4 ppt) during nighttime, resulting in the observed $ClNO_2$ production even under lower turbulence conditions. We explored the loss of NO_3 to reaction with VOCs (e.g. **R6**) using a box numerical model (*Sect. S1*, **Fig. S14**). These modeling results show that during the four case nights, which

had varying temperatures, friction velocities, and ground cover (**Fig. 3, Table S2**), NO_3 is simulated to be lost primarily through formation of $ClNO_2$ and HNO_3 (**Fig. S14**), rather than reaction with VOCs.

In contrast to its precursor N_2O_5, $ClNO_2$ shows significantly higher ($p<0.05$, t-test) average mole ratios under lower turbulence ($u^*<0.1$ m s^{-1}) conditions at 21:30, 22:00, 23:00, and 07:00 (**Fig. 4b**). These statistically significant time periods correspond to an average 6.3 times higher $ClNO_2$ mole ratio during lower turbulence conditions, in comparison to higher turbulence conditions. Considering the entire period of 21:30-07:30, $ClNO_2$ mole ratios were 3.6 times higher, on average, during lower turbulence conditions in comparison to higher turbulence conditions. Considering the nighttime period as a whole (18:00-08:00), $ClNO_2$ mole ratios were higher by 7±1 ppt (2.6-fold) during lower turbulence, in comparison to higher turbulence conditions.

In summary, average N_2O_5 mole ratios were significantly higher ($p<0.05$) at six different 30 min time periods, corresponding to 5.9 times higher N_2O_5 mole ratios during higher turbulence conditions, in comparison to lower turbulence conditions. The reduced N_2O_5 mole ratios observed under lower turbulence conditions are likely due to the short lifetime of NO_3 (N_2O_5 precursor, R3) when vehicle NO_x is emitted into the stable boundary layer, as observed in previous studies (Brown et al., 2007; Wang et al., 2006). However, average $ClNO_2$ mole ratios were significantly higher ($p<0.05$) during four different 30 min time periods, corresponding to 6.3 times higher $ClNO_2$ mole ratios during lower turbulence conditions, in comparison to higher turbulence conditions. This points to a likely surface source of $ClNO_2$ upon surface deposition of N_2O_5. Therefore, in Section 3.4, we investigated the influence of ground cover (Section 3.4).

3.4 Effects of ground cover

There were no statistically significant ($p<0.05$, t-test) differences in the average abundances of N_2O_5 over the diel period for snow-covered vs bare ground (**Fig. 5a**). This is consistent with measurements of similar net negative (deposition) fluxes of N_2O_5 over both snow-covered and bare ground (McNamara et al., 2021). The nighttime average mole ratios of N_2O_5 were 70±5 ppt and 68±4 ppt over snow-covered and bare ground, respectively. In contrast, **Figure 5b** shows significantly higher ($p<0.05$, t-test) average $ClNO_2$ mole ratios observed over snow-covered ground at 19:30-22:00, 23:00-

00:00, 01:00-01:30, 03:00, and 07:30. These statistically significant time points correspond to, on average, 3.5 times higher $ClNO_2$ mole ratios over snow-covered ground, in comparison to bare ground. Considering the entire period of 19:30-07:30, $ClNO_2$ mole ratios were 2.8 times higher, on average, over snow covered ground in comparison to bare ground. This is consistent with measurements of typical net positive (production) fluxes of $ClNO_2$ over snow-covered ground, and with field-based chamber experiments showing that $ClNO_2$ can be produced from the reaction of N_2O_5 on the saline snowpack (McNamara et al., 2021). The nighttime average mole ratios of $ClNO_2$ were 14.9±0.8 ppt and 7.0±0.5 ppt over snow-covered and bare ground, respectively.

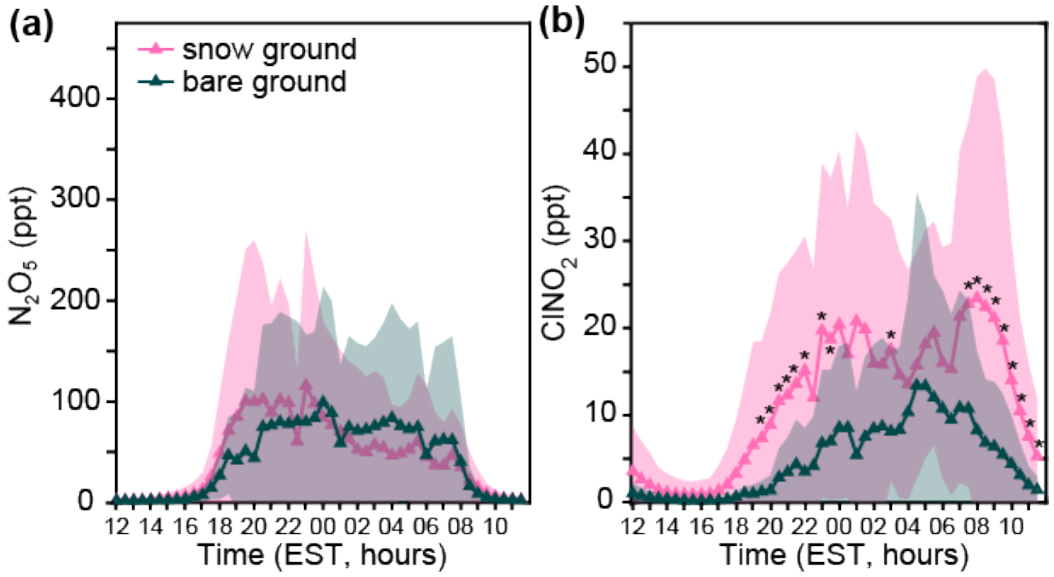

Figure 5. Diel patterns of 30 min averaged mole ratios of (a) N_2O_5 and (b) $ClNO_2$ binned by snow-covered and bare ground conditions from January 20 to February 24. Shading represents one standard deviation. Asterisks represent statistically significant (t-test) differences at the $p < 0.05$ level between snow-covered and bare ground for each 30 min time period. The ground was snow-covered 57% [20 d] of the study and was bare for 43% [15 d] of the study.

To summarize, there were no statistically significant ($p<0.05$) differences in average N_2O_5 mole ratios over the diel period for snow-covered versus bare ground. Yet, significantly higher ($p<0.05$) average $ClNO_2$ mole ratios were observed over snow-covered ground for 11 (of 28) nighttime 30 min time periods, corresponding to 3.5 times higher $ClNO_2$ mole ratios over snow-covered ground, in comparison to bare ground. During the same field campaign, net positive (production) fluxes of $ClNO_2$ were measured over snow-covered ground, and field-based chamber experiments showed that $ClNO_2$ can

be produced from the reaction of N_2O_5 on the saline snowpack (McNamara et al., 2021). The observed enhancement of $ClNO_2$ over snow-covered ground results herein suggests that snowpack $ClNO_2$ production was a frequent and significant occurrence across the field campaign (e.g. enough to influence the campaign-wide average results). We investigate the effects of other parameters (e.g. $PM_{2.5}$ Cl^-, NO_3^-, temperature, relative humidity, O_3 concentration, aerosol surface area, and pressure) in Section 3.5.

3.5 Competing effects of environmental conditions

Many of the environmental conditions discussed (precipitation/fog, turbulence regimes, and snow-covered/bare ground) occur simultaneously, and as a result, are difficult to discuss in isolation. Higher mole ratios of N_2O_5 were observed under higher turbulence conditions ($u^* > 0.25$ m s^{-1}) (Section 3.3), which occurred most frequently (67%) over bare ground (**Fig. S3**). In contrast, higher mole ratios of $ClNO_2$ were observed under lower turbulence conditions ($u^* < 0.25$ m s^{-1}) (Section 3.3), which occurred most frequently (73%) over snow-covered ground (**Fig. S3**). For select nights when vertical profile experiments were conducted by McNamara et al. (2021) during the same campaign, no statistically significant difference ($p = 0.48$) was observed for N_2O_5 deposition fluxes over bare ground versus snow-covered ground. Lower turbulence ($u^*<0.1$ m s^{-1}) and snow-covered ground were observed simultaneously for 24%, 48%, 26%, and 2% of the time during clear, snowfall, fog, and rainfall conditions, respectively (**Fig. S3**). The prevalence of lower turbulence and snow-covered ground during snowfall likely also contributes to the result that mole ratios of $ClNO_2$ were highest on average during snowfall (**Fig. 2**). These trends are consistent with snowpack $ClNO_2$ production, as also evidenced by the positive (upward) $ClNO_2$ fluxes observed over snow-covered ground and negative (downward) $ClNO_2$ fluxes observed over bare ground, during separate vertical profile experiments during the same campaign McNamara et al. (2021).

Given that multiple environmental factors that control N_2O_5 and $ClNO_2$ mole ratios are changing across the various weather conditions, we used a box numerical model, described in Section S1, to explore the variations in N_2O_5 and $ClNO_2$ abundances that can be attributed to changes in temperature, pressure, O_3 mole ratios, and aerosol surface area across the four case study nights. This numerical model does not consider the impacts of fog, rainfall, snowfall, ground cover, turbulence, or advection. Note that no

relationship was observed between wind direction or wind speed and mole ratios of N_2O_5 or $ClNO_2$ (**Fig. S13**), suggesting limited advection influence. Further, under the low wind speed conditions of the campaign (nighttime median=1.0 m s^{-1}), the gas mole ratios are expected to be higher in response to decreased atmospheric dispersion of gases and emissions/deposition from nearby sources/sinks. Therefore, we mainly attribute differences between calculated and measured N_2O_5 and $ClNO_2$ abundances primarily to the effects of non-parameterized meteorological processes (e.g., wet deposition and fog droplet scavenging). The model results (**Fig. 6, S14-16**) are discussed in detail in Section S2. Importantly, we conclude that variations in temperature, pressure, O_3 mole ratios, and aerosol surface area between the different case studies are insufficient to explain the significant differences in N_2O_5 and $ClNO_2$ mole ratios observed between these case study nights and point to the importance of other processes, including scavenging, discussed in this manuscript.

For the clear snowfall, fog, and rainfall case study nights, simulated N_2O_5 mole ratios averaged 150 ppt, 190 ppt, 140 ppt, and 380 ppt, respectively, during the last 4 h of the simulation (hours 10-14, 04:00-08:00 EST, to account for model spin-up and stabilization) (**Fig. 6**). In comparison, the maximum observed N_2O_5 mole ratios were 274 ppt, 34.2 ppt, 2.7 ppt, and 11.4 ppt from 04:00-08:00 EST during the clear, snowfall, fog, and rainfall cases respectively (**Fig. 6**). While plausible scenarios of [NO_2] and N_2O_5 uptake could simulate the observed N_2O_5 mole ratios (**Fig. S15**), the model scenario corresponding to previous work in wintertime Ann Arbor, MI (McNamara et al., 2020) underpredicts the average N_2O_5 mole ratio (229 ppt) by 42% . However, in contrast, the model drastically over-predicted N_2O_5 mole ratios for both the fog case (by ~50 times) and rainfall case (by ~30 times), and also over-predicted N_2O_5 mole ratios during the snowfall case (by ~5 times). As discussed in Section S2, realistic model conditions could not simulate the observed N_2O_5 mole ratios for the fog, rainfall, and snowfall cases. This supports scavenging as a missing N_2O_5 sink, with this being most significant during fog and rainfall, and potentially also contributing during snowfall.

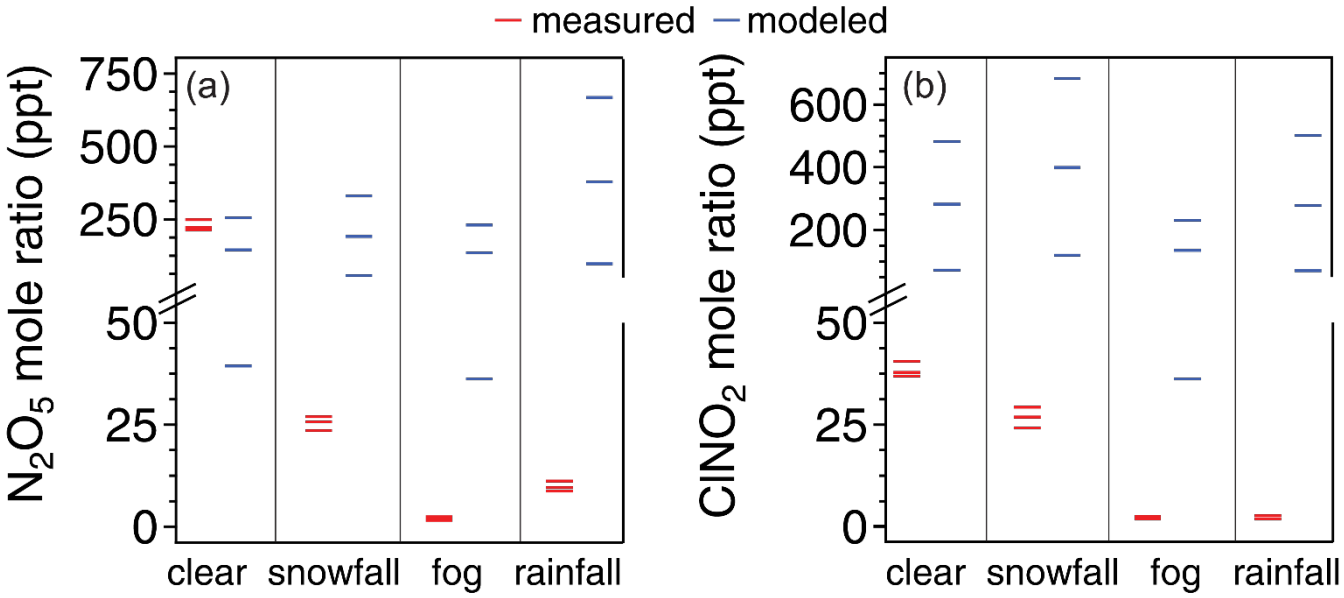

Figure 6: A comparison of measured (red) vs modeled (blue) mole ratios of N_2O_5 (a) and $ClNO_2$ (b) for each case study night. For measured values, the minimum, average, and maximum mole ratios from 04:00 – 08:00 EST of each case study (Fig. 3) are shown. For modeled values, the average mole ratios from the last 4 h of each 14 h simulation are shown; model inputs for the case studies are described in *Sect. S1*. Here, we hold the $\gamma^*\varphi$ product (N_2O_5 uptake*$ClNO_2$ yield) constant at 0.0037, and show the model outputs when $[NO_2]$ = 9.4 ppb, 31 ppb, and 59 ppb, respectively; $[NO_2]$ = 9.4 ppb produced the lowest modeled values of N_2O_5 and $ClNO_2$, and $[NO_2]$ = 59 ppb produced the highest modeled values of N_2O_5 and $ClNO_2$. For context, McNamara et al. (2020) previously reported a modeled median $[NO_2]$ of 31 ppb and $\gamma^*\varphi$ product constant of 0.0037 for wintertime Ann Arbor, MI.

Considering the entire SNACK field campaign, temperature was statistically significantly different between clear conditions and snowfall, fog, and rainfall, respectively ($p<0.05$, t-test) (**Fig. 7c**). The average nighttime temperatures were 265.8±0.2 K, 270.8±0.3 K, 276.7±0.2 K, and 282.1±0.2 K during snowfall, clear conditions, fog, and rainfall, respectively. Since lower temperatures favor N_2O_5 production in its thermal equilibrium (**R3**) (Asaf et al., 2010; Wagner et al., 2013), and because snowfall conditions had the lowest average temperature (**Fig. 7c**), we would expect N_2O_5 to be highest in abundance during snowfall if other processes did not dominate. In contrast, the measurements showed the highest average N_2O_5 mole ratios during clear conditions (**Fig. 2**), highlighting the importance of other effects, including wet scavenging. Further, as shown in the case study model simulations, discussed above, that did not consider scavenging, simulated N_2O_5 mole ratios were highest during the rainfall case

due to lower aerosol surface area concentrations, and second highest during the snowfall case because of the temperature effect (**Fig. 7**). Therefore, we conclude that temperature alone cannot explain the significant differences in N_2O_5 mole ratios between the clear, fog, rainfall, and snowfall conditions.

Relative humidity was also statistically significantly different between clear conditions and snowfall, fog, and rainfall, respectively ($p<0.05$) across the SNACK field campaign (**Fig. 7d**). The average nighttime RH values were 75.0±0.5%, 83.0±0.3%, 90.2±0.4%, and 93.7±0.3% during clear conditions, snowfall, rainfall, and fog, respectively. Higher RH typically increases N_2O_5 partitioning from the gas to aqueous phases (e.g. Osthoff et al., 2006; Sommariva et al., 2009; Wood et al., 2005). Indeed, the pattern of N_2O_5 abundance was anticorrelated with RH (**Fig. 2** and **Fig. 7d**). This reinforces that N_2O_5 heterogeneous uptake is strongly RH dependent (Bertram et al., 2009; Davis et al., 2008; Evans and Jacob, 2005; Griffiths and Cox, 2009; Hallquist et al., 2003), with enhanced uptake and removal occurring when RH and aerosol liquid water content are high.

The box model overestimated $ClNO_2$ mole ratios for the clear case (by ~6 times), despite lower simulated N_2O_5 mole ratios compared to modeled values (by ~42%) (**Fig. 6**), as discussed in the Section S2. Since the chosen values for [NO_2], N_2O_5 uptake, and $ClNO_2$ yield corresponded to previous work in wintertime Ann Arbor, MI (McNamara et al., 2020), this points to the variability and need to better constrain N_2O_5 uptake and $ClNO_2$ yield, as highlighted previously by McDuffie et al. (2018). However, realistic model conditions could be chosen to simulate the observed clear case N_2O_5 and $ClNO_2$ mole ratios (**Fig. S15 and S16**). In contrast to the clear case, realistic [NO_2], N_2O_5 uptake, and $ClNO_2$ yield values could not be chosen to simulate the observed $ClNO_2$ mole ratios, similar to the result for N_2O_5 mole ratios, discussed above. Average simulated $ClNO_2$ mole ratios were 400 ppt, 140 ppt, and 280 ppt for the snowfall, fog, and rainfall cases, respectively, during the last 4 h of the simulation (**Fig. 6**). In comparison, the maximum observed $ClNO_2$ mole ratios were 33.6 ppt, 2.5 ppt, and 3.2 ppt from 04:00-08:00 EST of the snowfall, fog, and rainfall cases, respectively (**Fig. 6**). Further, the model drastically overpredicted $ClNO_2$ mole ratios during the fog case (by ~50 times, similar to the N_2O_5 mole ratio overprediction) and rainfall case (by ~90 times, as compared to ~30 times over-prediction of N_2O_5 mole ratios), but also over-predicted $ClNO_2$ mole ratios during the snowfall case (by ~12 times, as compared to ~5 times for N_2O_5 mole ratios). The similar overprediction of N_2O_5 and $ClNO_2$ during fog supports fog

droplet scavenging of N_2O_5, in particular, as a missing sink in the model. The higher overprediction of $ClNO_2$ mole ratios, compared to N_2O_5, during the rainfall case, in particular, suggests that $ClNO_2$, in addition to N_2O_5, likely undergoes scavenging/wet deposition.

We also investigated N_2O_5 and $ClNO_2$ levels in the context of observed $PM_{2.5}$ Cl^- and NO_3^- concentrations. The averages for these parameters are given for clear conditions and each type of weather event in **Table 1**, with additional data provided in **Table S2**. As shown by Bertram and Thornton (2009), both N_2O_5 uptake and the product yield of $ClNO_2$ are expected to increase with increasing particulate chloride concentrations. The effects of increased particulate chloride are two-fold, with less N_2O_5 expected to remain in the gas-phase due to the increased uptake, and a higher $ClNO_2$ abundance expected because of the higher product yield. $PM_{2.5}$ Cl^- concentrations were not statistically significantly different between snowfall and clear conditions ($p=0.96$, t-test), between snowfall and rainfall ($p=0.11$), or between clear and rainfall conditions ($p=0.10$) (**Fig. 7a**).

$PM_{2.5}$ Cl^- concentrations were statistically significantly higher during fog, in comparison to clear conditions ($p<0.05$), with the average concentration during fog higher by 0.20±0.01 μg m^{-3} (1.8 times) on average. Although total submicron aerosol number concentrations were not statistically significantly different between clear and fog conditions ($p=0.88$), submicron aerosol surface area concentrations were significantly higher ($p<0.05$) during fog compared to clear conditions, by 52±7 μm^2 cm^{-3} (1.3 times) with respect to campaign averages (**Fig. S11-S12**). N_2O_5 uptake is expected to increase with increasing aerosol surface area concentration (Bertram and Thornton, 2009), but despite elevated $PM_{2.5}$ Cl^- and aerosol surface area concentrations during fog, average $ClNO_2$ abundance was lower during fog in comparison to clear conditions (**Fig. 2**). We expect that, during fog, elevated RH (**Fig. 7d**) has a greater impact on $ClNO_2$ abundance than $PM_{2.5}$ Cl^- concentration or aerosol surface area concentration. Production of particle-phase chloride, presumed to be from uptake of gas-phase HCl, has been observed previously during fog/haze events in highly polluted urban India (Gunthe et al., 2021) and near an incinerator (Johnson et al., 1987). However, for this study in Kalamazoo, MI, road salting seems more plausible as the dominant source of increased $PM_{2.5}$ Cl^- during wintertime fog.

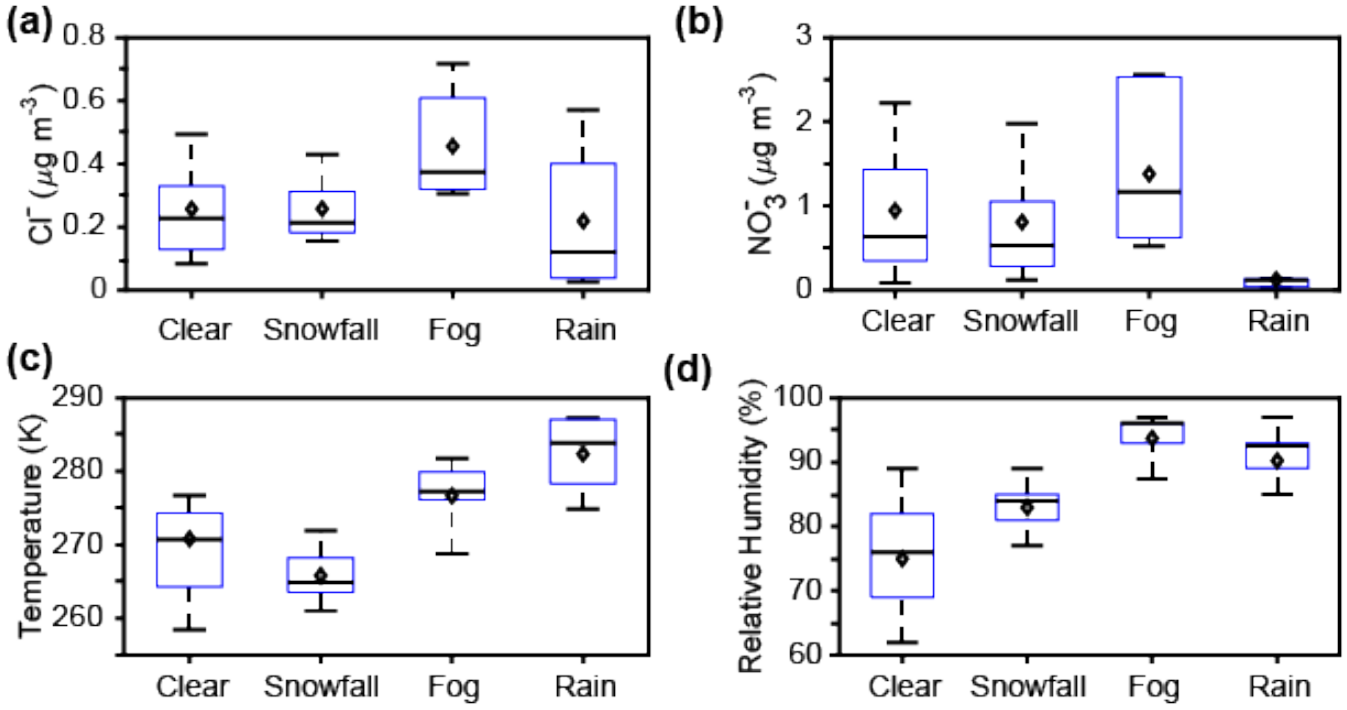

Figure 7. Box plots showing 30 min averaged $PM_{2.5}$ (a) chloride and (b) nitrate concentrations, (c) air temperatures and (d) relative humidity values during clear conditions and weather events (snowfall, fog, and rain). Bars represent the 10th, 50th, and 90th percentiles, boxes represent the 25th and 75th percentiles, and diamonds represent the means. Only nighttime data, between 18:00 and 08:00 EST, are included.

N_2O_5 uptake results in particulate nitrate production; however, the efficiency of N_2O_5 uptake to particles decreases with increasing particulate nitrate concentrations (Bertram and Thornton, 2009). $PM_{2.5}$ NO_3^- concentrations were not statistically significantly different between snowfall and clear conditions ($p=0.08$). $PM_{2.5}$ NO_3^- concentrations during rain were statistically significantly lower, in comparison to clear conditions ($p<0.05$), with average concentrations lower by 0.82±0.04 μg m^{-3} (7.5 times) (**Fig 6b**). This is attributed to increased scavenging and wet deposition of nitrate during rainfall, compared to snowfall, which is consistent with previous observations and calculations of scavenging coefficients for nitrate during rainfall and snowfall in winter in New York (Sperber and Hameed, 1986).

Particles rich in nitrate have been observed previously in the droplet mode (0.8–0.9 μm) during fog events; these particles form following fog droplet evaporation after nitrate production from HNO_3 and N_2O_5 uptake (Dall'Osto et al., 2009; Ge et al., 2012). In contrast to rain and snowfall, $PM_{2.5}$ NO_3^-

concentrations were statistically significantly higher during fog, in comparison to clear conditions ($p<0.05$), by 0.43±0.06 μg m^{-3} (160±20 ppt; 1.5 times) (**Figs. 6b** and **S10**). The increase in $PM_{2.5}$ NO_3^- is likely, in part, the result of heterogeneous uptake and hydrolysis of N_2O_5 (Brown et al., 2004; Osthoff et al., 2006), consistent with our observation of the lower average N_2O_5 mole ratios during fog (**Fig. 2**). On average, N_2O_5 was 76±5 ppt lower during fog compared to clear conditions (**Figs. 2** and **S10**). While this difference is not completely attributable to N_2O_5 uptake, it would correspond to a nitrate concentration of 0.21 μg m^{-3}. In addition to N_2O_5, gas-phase HNO_3 uptake likely also contributed to the increased $PM_{2.5}$ NO_3^- observed during fog. Due to its high solubility, HNO_3 is predicted to be efficiently scavenged by fog droplets (>90-100% removal) (Ervens, 2015). However, due to the limited HNO_3 data available (**Fig. S9**), a quantitative evaluation of HNO_3 contribution to nitrate production was not possible. It is likely that both N_2O_5 and HNO_3 uptake, followed by aqueous-phase nitrate formation, led to the increased $PM_{2.5}$ NO_3^- observed during fog.

4 Conclusions

We examined the impacts of precipitation (rain, snowfall) and fog, atmospheric turbulence, and ground cover (snow-covered vs bare) on near-surface (~1.5 m above ground) N_2O_5 and $ClNO_2$ observed during January to February 2018 in Kalamazoo, Michigan. While N_2O_5 was observed during all nights of the campaign, N_2O_5 mole ratios were lowest during periods of lower turbulence ($u^*<0.1$ m s^{-1}) due to titration of NO_3 and O_3 by NO in the stable nocturnal boundary layer. N_2O_5 mole ratios were not statistically significantly different over bare versus snow-covered ground. $ClNO_2$ mole ratios were highest during periods of lower turbulence and snow-covered ground. This is consistent with N_2O_5 depositing and reacting with the chloride-containing snowpack to produce $ClNO_2$. Indeed, vertical gradient measurements during the same study showed N_2O_5 deposition and an average positive (production) $ClNO_2$ flux over snow-covered ground, and snow chamber experiments showed that synthesized N_2O_5 reacted with the local saline snow to produce $ClNO_2$ (McNamara et al., 2021). This finding is also consistent with the laboratory study by Lopez-Hilfiker et al. (2012), which showed that N_2O_5 can react on halide-doped ice surfaces to produce $ClNO_2$. The contribution of the snowpack as a common $ClNO_2$

source across the field campaign has important implications for the vertical distribution of atmospheric chlorine chemistry, which will be examined in a future manuscript through one-dimensional modeling for comparison with chloride-containing aerosol particles that serve as a major $ClNO_2$ source.

On average, both N_2O_5 and $ClNO_2$ abundances were lowest during rainfall and fog due to scavenging. While both species are water soluble, N_2O_5 undergoes more efficient scavenging by liquid droplets, particularly fog, as expected based on its higher Henry's Law constant and uptake coefficient (Fickert et al., 1998; Gržinić et al., 2017). N_2O_5 uptake by fog droplets likely contributed to observed elevated $PM_{2.5}$ NO_3^- during fog events. Little is known about N_2O_5 and $ClNO_2$ scavenging by precipitation, supporting the need for further investigation of this process. Overall, our results show that observational and modeling studies of only clear conditions miss important processes including scavenging, fog nitrate production, and the snowpack as a $ClNO_2$ source. This is important as rainfall, fog, and snowfall occurred during 28% of the nighttime periods, representing a significant portion that contributes significantly to the variability observed during this winter study.

Acknowledgements

This study was supported by the US National Science Foundation Atmospheric Chemistry program (AGS-1738588 and PLR-1417914), an Alfred P. Sloan Foundation Research Fellowship in Chemistry, and the University of Michigan. J.E. acknowledges funding from the Swiss National Science Foundation (155999). We thank Andrew Ault, Nicholas Ellsworth, and Matthew McNamara for assistance in preparing the mobile laboratory, Angela Raso, Peter Peterson, Guy Burke, and Alexa Watson for fieldwork assistance, and Western Michigan University for use of their facilities for this study.

Data Availability

The CIMS and AIM-IC datasets are archived through PANGAEA: Kulju, Kathryn; Pratt, Kerri A (2021): N_2O_5, $ClNO_2$, $PM_{2.5}$ chloride, and $PM_{2.5}$ nitrate in Kalamazoo, Michigan, USA during January-February 2018. PANGAEA, 2021, https://doi.org/10.1594/PANGAEA.933765.

Author Contributions

KK wrote the manuscript, with feedback from all coauthors. KP designed the study, and SM and JE conducted the measurements and calibrations. KK led data analysis and interpretation, with contributions from SM, JE, QC, JDF, and KP. HK and KK completed the box modeling. JDF assisted with the air turbulence measurements and analysis, in particular. SB coordinated logistics at the field site.

Competing Interests

The authors declare that they have no conflict of interest.

References

Allan, B. J., Carslaw, N., Coe, H., Burgess, R. A. and Plane, J. M. C.: Observations of the nitrate radical in the marine boundary layer, J. Atmos. Chem., 33(2), 129–154, doi:10.1023/A:1005917203307, 1999.

Asaf, D., Tas, E., Pedersen, D., Peleg, M. and Luria, M.: Long-term measurements of NO_3 radical at a semiarid urban site: 2. Seasonal trends and loss mechanisms, Environ. Sci. Technol., 44(15), 5901–5907, doi:10.1021/es100967z, 2010.

Behnke, W., George, C., Scheer, V. and Zetzsch, C.: Production and decay of $ClNO_2$ from the reaction of gaseous N_2O_5 with NaCl solution: Bulk and aerosol experiments, J. Geophys. Res., 102, 3795–3804, doi:10.1029/96JD03057, 1997.

Bertram, T. H. and Thornton, J. A.: Toward a general parameterization of N_2O_5 reactivity on aqueous particles: the competing effects of particle liquid water, nitrate and chloride, Atmos. Chem. Phys., 9, 8351–8363, doi:10.5194/acp-9-8351-2009, 2009.

Bertram, T. H., Thornton, J. A., Riedel, T. P., Middlebrook, A. M., Bahreini, R., Bates, T. S., Quinn, P. K. and Coffman, D. J.: Direct observations of N_2O_5 reactivity on ambient aerosol particles, Geophys. Res. Lett., 36(19), 1–5, doi:10.1029/2009GL040248, 2009.

Brown, S. S., Dibb, J. E., Stark, H., Aldener, M., Vozella, M., Whitlow, S., Williams, E. J., Lerner, B. M., Jakoubek, R., Middlebrook, A. M., DeGouw, J. A., Warneke, C., Goldan, P. D., Kuster, W. C.,

Angevine, W. M., Sueper, D. T., Quinn, P. K., Bates, T. S., Meagher, J. F., Fehsenfeld, F. C. and Ravishankara, A. R.: Nighttime removal of NO_x in the summer marine boundary layer, Geophys. Res. Lett., 31(7), 2–6, doi:10.1029/2004GL019412, 2004.

Brown, S. S., Dubé, W. P., Osthoff, H. D., Stutz, J., Ryerson, T. B., Wollny, A. G., Brock, C. A., Warneke, C., de Gouw, J. A., Atlas, E., Neuman, J. A., Holloway, J. S., Lerner, B. M., Williams, E. J., Kuster, W. C., Goldan, P. D., Angevine, W. M., Trainer, M., Fehsenfeld, F. C. and Ravishankara, A. R.: Vertical profiles in NO_3 and N_2O_5 measured from an aircraft: Results from the NOAA P-3 and surface platforms during the New England Air Quality Study 2004, J. Geophys. Res. Atmos., 112(22), 1–17, doi:10.1029/2007JD008883, 2007.

Brown, S. S., Dubé, W. P., Tham, Y. J., Zha, Q., Xue, L., Poon, S., Wang, Z., Blake, D. R., Tsui, W., Parrish, D. D. and Wang, T.: Nighttime chemistry at a high altitude site above Hong Kong, J. Geophys. Res. Atmos., (3), 2457–2475, doi:10.1002/2015JD024566.Received, 2016.

Chang, W. L., Bhave, P. V, Brown, S. S., Riemer, N., Stutz, J. and Dabdub, D.: Heterogeneous Atmospheric Chemistry, Ambient Measurements, and Model Calculations of N_2O_5: A Review, Aerosol Sci. Technol., 45(6), 665–695, doi:10.1080/02786826.2010.551672, 2011.

Chen, Q., Edebeli, J., McNamara, S. M., Kulju, K. D., May, N. W., Bertman, S. B., Thanekar, S., Fuentes, J. D. and Pratt, K. A.: HONO, Particulate Nitrite, and Snow Nitrite at a Midlatitude Urban Site during Wintertime, ACS Earth Sp. Chem., 3(5), 811–822, doi:10.1021/acsearthspacechem.9b00023, 2019.

Christiansen, A., Carlton, A. and Henderson, B.: Differences in Fine Particle Chemical Composition on Clear and Cloudy Days, Atmos. Chem. Phys., (March), 1–26, doi:10.5194/acp-2020-184, 2020.

Crutzen, P. J.: The Role of NO and NO_2 in the Chemistry of the Troposphere and Stratosphere, Ann. Rev. Earth Planet. Sci., 7, 443–72, doi:10.1146/annurev.ea.07.050179.002303, 1979.

Dall'Osto, M., Harrison, R. M., Coe, H. and Williams, P.: Real-time secondary aerosol formation during a fog event in London, Atmos. Chem. Phys., 9(7), 2459–2469, doi:10.5194/acp-9-2459-2009, 2009.

Davis, J. M., Bhave, P. V. and Foley, K. M.: Parameterization of N_2O_5 reaction probabilities on the surface of particles containing ammonium, sulfate, and nitrate, Atmos. Chem. Phys., 8(17), 5295–5311, doi:10.5194/acp-8-5295-2008, 2008.

Evans, M. J. and Jacob, D. J.: Impact of new laboratory studies of N_2O_5 hydrolysis on global model

budgets of tropospheric nitrogen oxides, ozone, and OH, Geophys. Res. Lett., 32(9), 1–4, doi:10.1029/2005GL022469, 2005.

Fickert, S., Helleis, F., Adams, J. W., Moortgat, G. K. and Crowley, J. N.: Reactive uptake of $ClNO_2$ on aqueous bromide solutions, J. Phys. Chem. A, 102(52), 10689–10696, doi:10.1021/jp983004n, 1998.

Finlayson-Pitts, B. J. . and Pitts, J. N. .: Formation of chemically active chlorine compounds by reactions of atmospheric NaCl particles with gaseous N_2O_5 and $ClONO_2$, Nature, 337(6204), 241–244, doi:10.1038/337241a0, 1989.

Frenzel, A., Scheer, V., Sikorski, R., George, C., Behnke, W. and Zetzsch, C.: Heterogeneous interconversion reactions of BrNO2, ClNO2, Br2, and Cl2, J. Phys. Chem. A, 102(8), 1329–1337, doi:10.1021/jp973044b, 1998.

Ge, X., Zhang, Q., Sun, Y., Ruehl, C. R. and Setyan, A.: Effect of aqueous-phase processing on aerosol chemistry and size distributions in Fresno, California, during wintertime, Environ. Chem., 9(3), 221–235, doi:10.1071/EN11168, 2012.

Geyer, A., Alicke, B., Konrad, S., Schmitz, T., Stutz, J. and Platt, U.: Chemistry and oxidation capacity of the nitrate radical in the continental boundary layer near Berlin, J. Geophys. Res. Atmos., 106(D8), 8013–8025, doi:10.1029/2000JD900681, 2001.

Griffiths, P. T. and Cox, R. A.: Temperature dependence of heterogeneous uptake of N_2O_5 by ammonium sulfate aerosol, Atmos. Sci. Lett., 10, 159–163, doi:10.1002/asl.225, 2009.

Gržinić, G., Bartels-Rausch, T., Türler, A. and Ammann, M.: Efficient bulk mass accommodation and dissociation of N_2O_5 in neutral aqueous aerosol, Atmos. Chem. Phys., 17(10), 6493–6502, doi:10.5194/acp-17-6493-2017, 2017.

Gunthe, S. S., Liu, P., Panda, U., Raj, S. S., Sharma, A., Darbyshire, E., Reyes-Villegas, E., Allan, J., Chen, Y., Wang, X., Song, S., Pöhlker, M. L., Shi, L., Wang, Y., Kommula, S. M., Liu, T., Ravikrishna, R., McFiggans, G., Mickley, L. J., Martin, S. T., Pöschl, U., Andreae, M. O. and Coe, H.: Enhanced aerosol particle growth sustained by high continental chlorine emission in India, Nat. Geosci., 14(2), 77–84, doi:10.1038/s41561-020-00677-x, 2021.

Hallquist, M., Stewart, D. J., Stephenson, S. K. and Cox, R. A.: Hydrolysis of N_2O_5 on sub-micron sulfate aerosols, Phys. Chem. Chem. Phys., 5(16), 3453–3463, doi:10.1039/b301827j, 2003.

Heintz, F., Platt, U., Flentje, H. and Dubois, R.: Long-term observation of nitrate radicals at the Tor Station, Kap Arkona (Rügen), J. Geophys. Res., 101(D17), 22891–22910, 1996.

Huey, L. G., Tanner, D. J., Slusher, D. L., Dibb, J. E., Arimoto, R., Chen, G., Davis, D., Buhr, M. P., Nowak, J. B., Mauldin, R. L., Eisele, F. L. and Kosciuch, E.: CIMS measurements of HNO_3 and SO_2 at the South Pole during ISCAT 2000, Atmos. Environ., 38, 5411–5421, doi:10.1016/j.atmosenv.2004.04.037, 2004.

Jacob, J.: Chemistry of OH in Remote Clouds and Its Role in the Production of Formic Acid and Peroxymonosulfate, , 91, 9807–9826, 1986.

Johnson, C. A., Sigg, L. and Zobrist, J.: Case studies on the chemical composition of fogwater: The influence of local gaseous emissions, Atmos. Environ., 21(11), 2365–2374, doi:10.1016/0004-6981(87)90371-4, 1987.

Kercher, J. P., Riedel, T. P. and Thornton, J. A.: Chlorine activation by N_2O_5: simultaneous, in situ detection of $ClNO_2$ and N_2O_5 by chemical ionization mass spectrometry, Atmos. Meas. Tech, 2, 193–204, doi:10.5194/amt-2-193-2009, 2009.

Leblanc, T. and Hauchecorne, A.: Recent observations of mesospheric temperature inversions, J. Geophys. Res. Atmos., 102(D16), 19471–19482, doi:10.1029/97JD01445, 1997.

Liao, J., Sihler, H., Huey, L. G., Neuman, J. A., Tanner, D. J., Friess, U., Platt, U., Flocke, F. M., Orlando, J. J., Shepson, P. B., Beine, H. J., Weinheimer, A. J., Sjostedt, S. J., Nowak, J. B., Knapp, D. J., Staebler, R. M., Zheng, W., Sander, R., Hall, S. R. and Ullmann, K.: A comparison of Arctic BrO measurements by chemical ionization mass spectrometry and long path-differential optical absorption spectroscopy, J. Geophys. Res. Atmos., 116, 1–14, doi:10.1029/2010JD014788, 2011.

Lillis, D., Cruz, C. N., Collett, J., Willard Richards, L. and Pandis, S. N.: Production and removal of aerosol in a polluted fog layer: Model evaluation and fog effect on PM, Atmos. Environ., 33(29), 4797–4816, doi:10.1016/S1352-2310(99)00264-2, 1999.

Lopez-Hilfiker, F. D., Constantin, K., Kercher, J. P. and Thornton, J. A.: Temperature dependent halogen activation by N_2O_5 reactions on halide-doped ice surfaces, Atmos. Chem. Phys, 12, 5237–5247, doi:10.5194/acp-12-5237-2012, 2012.

Markovic, M. Z., Vandenboer, T. C. and Murphy, J. G.: Characterization and optimization of an online

system for the simultaneous measurement of atmospheric water-soluble constituents in the gas and particle phases, J. Environ. Monit., 14, 1872–1884, doi:10.1039/c2em00004k, 2012.

McDuffie, E. E., Fibiger, D. L., Dubé, W. P., Lopez Hilfiker, F., Lee, B. H., Jaeglé, L., Guo, H., Weber, R. J., Reeves, J. M., Weinheimer, A. J., Schroder, J. C., Campuzano-Jost, P., Jimenez, J. L., Dibb, J. E., Veres, P., Ebben, C., Sparks, T. L., Wooldridge, P. J., Cohen, R. C., Campos, T., Hall, S. R., Ullmann, K., Roberts, J. M., Thornton, J. A. and Brown, S. S.: $ClNO_2$ Yields From Aircraft Measurements During the 2015 WINTER Campaign and Critical Evaluation of the Current Parameterization, J. Geophys. Res. Atmos., 123(22), 12,994-13,015, doi:10.1029/2018JD029358, 2018.

McNamara, S. M., W. Raso, A. R., Wang, S., Thanekar, S., Boone, E. J., Kolesar, K. R., Peterson, P. K., Simpson, W. R., Fuentes, J. D., Shepson, P. B. and Pratt, K. A.: Springtime Nitrogen Oxide-Influenced Chlorine Chemistry in the Coastal Arctic, Environ. Sci. Technol., 53, 8057–8067, doi:10.1021/acs.est.9b01797, 2019.

McNamara, S. M., Kolesar, K. R., Wang, S., Kirpes, R. M., May, N. W., Gunsch, M. J., Cook, R. D., Fuentes, J. D., Hornbrook, R. S., Apel, E. C., China, S., Laskin, A. and Pratt, K. A.: Observation of Road Salt Aerosol Driving Inland Wintertime Atmospheric Chlorine Chemistry, ACS Cent. Sci., 5, doi:10.1021/acscentsci.9b00994, 2020.

McNamara, S. M., Chen, Q., Edebeli, J., Kulju, K. D., Mumpfield, J., Fuentes, J. D., Bertman, S. B. and Pratt, K. A.: Observation of N2O5 deposition and ClNO2 production on the saline snowpack, ACS Earth Sp. Chem., doi:10.1021/acsearthspacechem.0c00317, 2021.

Mielke, L. H., Furgeson, A. and Osthoff, H. D.: Observation of $ClNO_2$ in a Mid-Continental Urban Environment, Environ. Sci. Technol, 45, 8889–8896, doi:10.1021/es201955u, 2011.

Monin, A. S. and Obukhov, A. M.: Basic laws of turbulent mixing in the surface layer of the atmosphere. [online] Available from: https://gibbs.science/teaching/efd/handouts/monin_obukhov_1954.pdf (Accessed 31 May 2019), 1954.

Neuman, J. A., Huey, L. G., Dissly, R. W., Fehsenfeld, F. C., Flocke, F., Holecek, J. C., Holloway, J. S., Hübler, G., Jakoubek, R., Nicks, D. K., Parrish, D. D., Ryerson, T. B., Sueper, D. T. and Weinheimer, A. J.: Fast-response airborne in situ measurements of HNO_3 during the Texas 2000 Air Quality Study,

J. Geophys. Res. D Atmos., 107, 1–12, doi:10.1029/2001JD001437, 2002.

Osthoff, H. D., Sommariva, R., Baynard, T., Pettersson, A., Williams, E. J., Lerner, B. M., Roberts, J. M., Stark, H., Goldan, P. D., Kuster, W. C., Bates, T. S., Coffman, D., Ravishankara, A. R. and Brown, S. S.: Observation of daytime N_2O_5 in the marine boundary layer during New England Air Quality Study - Intercontinental Transport and Chemical Transformation 2004, J. Geophys. Res. Atmos., 111(23), 1–13, doi:10.1029/2006JD007593, 2006.

Osthoff, H. D., Roberts, J. M., Ravishankara, A. R., Williams, E. J., Lerner, B. M., Sommariva, R., Bates, T. S., Coffman, D., Quinn, P. K., Dibb, J. E., Stark, H., Burkholder, J. B., Talukdar, R. K., Meagher, J., Fehsenfeld, F. C. and Brown, S. S.: High levels of nitryl chloride in the polluted subtropical marine boundary layer, Nat. Geosci., 1, 324–328, doi:10.1038/ngeo177, 2008.

Osthoff, H. D., Odame-ankrah, C. A., Tokarek, T. W., Taha, Y. M. and Corinne, L.: Low Levels of Nitryl Chloride in the Lower Fraser Valley of British Columbia, Atmos. Chem. Phys., 18(2), 6293–6315, 2018.

Phillips, G. J., Tang, M. J., Thieser, J., Brickwedde, B., Schuster, G., Bohn, B., Lelieveld, J. and Crowley, J. N.: Significant concentrations of nitryl chloride observed in rural continental Europe associated with the influence of sea salt chloride and anthropogenic emissions, Geophys. Res. Lett., 39(10), 1–5, doi:10.1029/2012GL051912, 2012.

Pruppacher, H. R. and Klett, J. D.: Microphysics of Clouds and Precipitation, 2nd ed., 1997.

Riedel, T. P., Wagner, N. L., Dubé, W. P., Middlebrook, A. M., Young, C. J., Öztürk, F., Bahreini, R., Vandenboer, T. C., Wolfe, D. E., Williams, E. J., Roberts, J. M., Brown, S. S. and Thornton, J. A.: Chlorine activation within urban or power plant plumes: Vertically resolved $ClNO_2$ and Cl_2 measurements from a tall tower in a polluted continental setting, J. Geophys. Res. Atmos., 118, 8702–8715, doi:10.1002/jgrd.50637, 2013.

Roberts, J. M., Osthoff, H. D., Brown, S. S., Ravishankara, A. R., Coffman, D., Quinn, P. and Bates, T.: Laboratory studies of products of N_2O_5 uptake on Cl- containing substrates, Geophys. Res. Lett., 36(20), 1–5, doi:10.1029/2009GL040448, 2009.

Royer, H. M., Mitroo, D., Hayes, S. M., Haas, S. M., Pratt, K. A., Blackwelder, P. L., Gill, T. E. and Gaston, C. J.: The role of hydrates, competing chemical constituents, and surface composition on

ClNO2formation, Environ. Sci. Technol., 55(5), 2869–2877, doi:10.1021/acs.est.0c06067, 2021.

Sander, R.: Compilation of Henry's law constants (version 4.0) for water as solvent, Atmos. Chem. Phys, 15, 4399–4981, doi:10.5194/acp-15-4399-2015, 2015.

Sarwar, G., Simon, H., Xing, J. and Mathur, R.: Importance of tropospheric $ClNO_2$ chemistry across the Northern Hemisphere, Geophys. Res. Lett., 41(11), 4050–4058, doi:10.1002/2014GL059962, 2014.

Simpson, W. R., Brown, S. S., Saiz-Lopez, A., Thornton, J. A. and Von Glasow, R.: Tropospheric Halogen Chemistry: Sources, Cycling, and Impacts, Chem. Rev., 115, 4035–4062, doi:10.1021/cr5006638, 2015.

Slusher, D. L., Huey, L. G., Tanner, D. J., Flocke, F. M. and Roberts, J. M.: A thermal dissociation - Chemical ionization mass spectrometry (TD-CIMS) technique for the simultaneous measurement of peroxyacyl nitrates and dinitrogen pentoxide, J. Geophys. Res. Atmos., 109(19), 1–13, doi:10.1029/2004JD004670, 2004.

Sommariva, R., Osthoff, H. D., Brown, S. S., Bates, T. S., Baynard, T., Coffman, D., De Gouw, J. A., Goldan, P. D., Kuster, W. C., Lerner, B. M., Stark, H., Warneke, C., Williams, E. J., Fehsenfeld, F. C., Ravishankara, A. R. and Trainer, M.: Radicals in the marine boundary layer during NEAQS 2004: A model study of day-time and night-time sources and sinks, Atmos. Chem. Phys., 9(9), 3075–3093, doi:10.5194/acp-9-3075-2009, 2009.

Stanier, C., Singh, A., Adamski, W., Baek, J., Caughey, M., Carmichael, G., Edgerton, E., Kenski, D., Koerber, M., Oleson, J., Rohlf, T., Lee, S. R., Riemer, N., Shaw, S., Sousan, S. and Spak, S. N.: Overview of the LADCO winter nitrate study: Hourly ammonia, nitric acid and $PM_{2.5}$ composition at an urban and rural site pair during $PM_{2.5}$ episodes in the US Great Lakes region, Atmos. Chem. Phys., 12(22), 11037–11056, doi:10.5194/acp-12-11037-2012, 2012.

Stull, R.: Practical Meteorology: An Algebra-based Survey of Atmospheric Science., 1.02b., Univ. of British Columbia. [online] Available from: https://www.eoas.ubc.ca/books/Practical_Meteorology/, 2017.

Stull, R. B.: An Introduction to Boundary Layer Meteorology., 1988.

Tham, Y. J., Wang, Z., Li, Q., Yun, H., Wang, W., Wang, X., Xue, L., Lu, K., Ma, N., Bohn, B., Li, X., Kecorius, S., Größ, J., Shao, M., Wiedensohler, A., Zhang, Y. and Wang, T.: Significant

concentrations of nitryl chloride sustained in the morning: investigations of the causes and impacts on ozone production in a polluted region of northern China, Atmos. Chem. Phys, 16, 14959–14977, doi:10.5194/acp-16-14959-2016, 2016.

Tham, Y. J., Wang, Z., Li, Q., Wang, W., Wang, X., Lu, K., Ma, N., Yan, C., Kecorius, S., Wiedensohler, A., Zhang, Y. and Wang, T.: Heterogeneous N_2O_5 uptake coefficient and production yield of $ClNO_2$ in polluted northern China: Roles of aerosol water content and chemical composition, Atmos. Chem. Phys., 18(17), 13155–13171, doi:10.5194/acp-18-13155-2018, 2018.

Thornton, J. A. and Abbatt, J. P. D.: N_2O_5 Reaction on Submicron Sea Salt Aerosol: Kinetics, Products, and the Effect of Surface Active Organics, J. Phys. Chem. A, 109, 10004–10012, doi:10.1021/jp054183t, 2005.

Thornton, J. A., Kercher, J. P., Riedel, T. P., Wagner, N. L., Cozic, J., Holloway, J. S., Dubé, W. P., Wolfe, G. M., Quinn, P. K., Middlebrook, A. M., Alexander, B. and Brown, S. S.: A large atomic chlorine source inferred from mid-continental reactive nitrogen chemistry, Nature, 464, 271–274, doi:10.1038/nature08905, 2010.

Wagner, N. L., Riedel, T. P., Young, C. J., Bahreini, R., Brock, C. A., Dubé, W. P., Kim, S., Middlebrook, A. M., Öztürk, F., Roberts, J. M., Russo, R., Sive, B., Swarthout, R., Thornton, J. A., VandenBoer, T. C., Zhou, Y. and Brown, S. S.: N_2O_5 uptake coefficients and nocturnal NO_2 removal rates determined from ambient wintertime measurements, J. Geophys. Res. Atmos., 118, 9331–9350, doi:10.1002/jgrd.50653, 2013.

Wang, S., Ackermann, R. and Stutz, J.: Vertical profiles of O_3 and NO_x chemistry in the polluted nocturnal boundary layer in Phoenix, AZ: I. Field observations by long-path DOAS, Atmos. Chem. Phys., 6(9), 2671–2693, doi:10.5194/acp-6-2671-2006, 2006.

Wang, S., McNamara, S. M., Kolesar, K. R., May, N. W., Fuentes, J. D., Cook, R. D., Gunsch, M. J., Mattson, C. N., Hornbrook, R. S., Apel, E. C. and Pratt, K. A.: Urban Snowpack $ClNO_2$ Production and Fate: A One-Dimensional Modeling Study, ACS Earth Sp. Chem., 4(7), 1140–1148, doi:10.1021/acsearthspacechem.0c00116, 2020.

Wang, X., Wang, H., Xue, L., Wang, T., Wang, L., Gu, R., Wang, W., Tham, Y. J., Wang, Z., Yang, L., Chen, J. and Wang, W.: Observations of N_2O_5 and $ClNO_2$ at a polluted urban surface site in North

China: High N_2O_5 uptake coefficients and low $ClNO_2$ product yields, Atmos. Environ., 156, 125–134, doi:10.1016/j.atmosenv.2017.02.035, 2017.

Wood, E. C., Bertram, T. H., Wooldridge, P. J. and Cohen, R. C.: Measurements of N_2O_5, NO_2, and O_3 east of the San Francisco Bay, Atmos. Chem. Phys., 4(5), 6645–6665, doi:10.5194/acp-5-483-2005, 2005.

Young, C. J., Washenfelder, R. A., Edwards, P. M., Parrish, D. D., Gilman, J. B., Kuster, W. C., Mielke, L. H., Osthoff, H. D., Tsai, C., Pikelnaya, O., Stutz, J., Veres, P. R., Roberts, J. M., Griffith, S., Dusanter, S., Stevens, P. S., Flynn, J., Grossberg, N., Lefer, B., Holloway, J. S., Peischl, J., Ryerson, T. B., Atlas, E. L., Blake, D. R. and Brown, S. S.: Chlorine as a primary radical: evaluation of methods to understand its role in initiation of oxidative cycles, Atmos. Chem. Phys, 14, 3427–3440, doi:10.5194/acp-14-3427-2014, 2014.

Supplement of:

Urban inland wintertime N_2O_5 and $ClNO_2$ influenced by ground cover, air turbulence, and precipitation

Kathryn D. Kulju[1], Stephen M. McNamara[1], Qianjie Chen[1†], Hannah S. Kenagy[1], Jacinta Edebeli[1,2], Jose D. Fuentes[3], Steven B. Bertman[4], Kerri A. Pratt[1,5*]

[1]Department of Chemistry, University of Michigan, Ann Arbor, MI 48109, USA
[2]Paul Scherrer Institut, 5232 Villigen, Switzerland
[3]Department of Meteorology and Atmospheric Science, Pennsylvania State University, University Park, Pennsylvania 16802, USA
[4]Institute of the Environment and Sustainability, Western Michigan University, Kalamazoo, Michigan 49008, USA
[5]Department of Earth and Environmental Sciences, University of Michigan, Ann Arbor, MI 48109, USA
[†]Current: Department of Civil and Environmental Engineering, Hong Kong Polytechnic University, Hong Kong

Correspondence to: Kerri A. Pratt (prattka@umich.edu)

S1. Box model details

A simple box model was used to explore the impacts of aerosol surface area, temperature, pressure, and [O_3] on N_2O_5 and $ClNO_2$ mole ratios for the case study nights. In addition, the model was used to explore the relative importance of VOCs on NO_3 loss (Fig S14). This model does not consider the impacts of fog, rainfall, snowfall, ground cover, turbulence, or advection. Note that no clear correlation was observed between N_2O_5 and $ClNO_2$ mole ratios and wind speed or wind direction (Fig. S13). Simulations were conducted over 14 h to examine the 18:00-08:00 EST nighttime period for each case night.). Temperature, pressure, and aerosol surface area (14.1-736.5 nm) (*Sections 2.1 and 2.4*) were set to be constant and equal to the observed averages from 18:00-08:00 EST for each case night (Table S3). The model was initialized with 0 ppt for NO_3, HNO_3, $ClNO_2$, and N_2O_5, and an initial O_3 mole ratio equal to the observed average from 18:00-08:00 EST for each case night (*Section 2.2*, Table S3). The initial NO mole ratio was set to be 20 ppt, with 10 ppt h^{-1} added to account for emissions from the contributions of vehicles from the nearby roadway; these values were chosen so that the modeled concentrations of NO_2 and O_3 were relatively stable throughout the 14 h simulations. When discussing the results of the simulation with respect to mole ratios of N_2O_5 and $ClNO_2$ for the case study nights (Fig S15-16), we discuss the average of the last 4 h of each simulation (i.e. 04:00-08:00); this was done to give the model time to reach steady state, at which point the results are less dependent on the initial conditions.

Following the approach of Kenagy et al. (2020), the model considers the following reactions, with rate constants from the Master Chemical Mechanism, MCM v 3.3.1 (Saunders et al., 2003):

$$NO + O_3 \rightarrow NO_2 + O_2 \quad \text{(R-S1)}$$
$$NO + NO_3 \rightarrow 2\,NO_2 \quad \text{(R-S2)}$$
$$NO_2 + O_3 + M \rightarrow O_2 + NO_3 \quad \text{(R-S3)}$$
$$NO_3 + VOCs \rightarrow products \quad \text{(R-S4)}$$
$$NO_2 + NO_3 + M \rightleftharpoons N_2O_5 \quad \text{(R-S5)}$$
$$N_2O_5 + H_2O \rightarrow 2HNO_3 \quad \text{(R-S6)}$$
$$N_2O_5 + Cl^- \rightarrow ClNO_2 + NO_3^- \quad \text{(R-S7)}$$

We use the reaction rate constant k_{hyd} for hydrolysis of N_2O_5 during its heterogeneous reaction (R-S6 and R-S7) and define it as follows based on Bertram and Thornton (2009):

$$k_{hyd} = \frac{\bar{c} \times S_a \times \gamma}{4} \quad \text{(E-S1)}$$

$\bar{c}$ is the temperature-dependent mean molecular speed of N_2O_5, S_a is the measured aerosol surface area concentration, and γ is the reactive uptake coefficient for N_2O_5.

To estimate the VOC reactivity to NO_3, we refer to previous measurements of light hydrocarbons (C_2H_6, C_3H_8, n-C_4H_{10}, i-C_4H_{10}, HCHO, and CH_3CHO) in Ann Arbor, MI during Feb. 2016 (McNamara et al., 2020). Considering the NO_3 rate constants reported by the National Institute of Standards and Technology kinetics database, we estimate the VOC reactivity to NO_3 to be 3.6×10^{-4} s^{-1}. Therefore, for the SNACK study the VOC reactivity to NO_3 was likely between 1×10^{-4} s^{-1} and 1×10^{-3} s^{-1}.

Since NO_2 was not measured in Kalamazoo, MI during the SNACK study, we refer to the previously simulated [NO_2] by Wang et al. (2020) using measured [NO] and [O_3] during February 2016 in Ann Arbor, MI. This previous study simulated a median nighttime [NO_2] of 31 ppb, with the 25th and 75th percentiles equal to 9.4 ppb and 59 ppb, respectively. Therefore, in the current study, we explore a [NO_2] range of 100 ppt – 100 ppb in our modeling (Fig S14-S16). We intentionally explore a larger range of VOC reactivity and [NO_2] than we expect was observed in wintertime MI, such that 1) the true conditions at the sampling site were likely captured and 2) the impacts of extreme conditions (e.g. very low VOC reactivity+very low [NO_2], very high VOC reactivity+very high [NO_2], etc.) are still shown such that the reader can see how those extreme conditions would influence our box model results.

The box model also includes N_2O_5 uptake (γ) and $ClNO_2$ yield (φ) onto aerosol particles (Bertram and Thornton, 2009). The average γ reported from Ann Arbor, MI in Feb – Mar 2016 was 0.0155, and the average φ was 0.24 ($\gamma\times\varphi$ product = 0.0037) (McNamara et al., 2020). Therefore, for the modeling herein, we explore a $\gamma\times\varphi$ product range of 0.0001 (10^{-4}, e.g. γ=0.001 and φ=0.1) – 0.01 (10^{-2}, e.g. γ=0.01 and φ=1) (Fig S14).

S2. Discussion of Box Model Results

As shown in Fig. S14, when $[NO_2]$ = 31 ppb (median during Feb. 2016 in Ann Arbor, MI (McNamara et al., 2020)), >95% of NO_3 is simulated to be lost through the inorganic pathways (production of HNO_3 and $ClNO_2$, compared to reaction with VOCs) for all VOC reactivities to NO_3 up to 10^{-3} s^{-1} and across all case studies (Fig S14). In fact, for all cases but one (rainfall), >95% of NO_3 is also lost through the inorganic pathways for VOC reactivities up to 10^{-3} s^{-1} at $[NO_2]$ = 9.4 ppb, which corresponds to the 25th percentile from another study in February 2016 in Ann Arbor, MI (McNamara et al., 2020). For the one exception (rainfall case), the 95th percentile for NO_3 lost through the inorganic pathways occurs at $[NO_2]$ = 16 ppb and at a VOC reactivity to NO_3 of 10^{-3} s^{-1}, with the 90th percentile occurring at $[NO_2]$ = 4.5 ppb. Therefore, we conclude that the VOC loss pathway for NO_3 is likely minor in this wintertime urban MI environment.

Since the model does not include fog, rainfall, or snowfall, we expect that the clear case study night should be best represented by the model. At NO_2 and $\gamma^*\varphi$ levels corresponding to Feb. 2016 in Ann Arbor, MI (NO_2=31 ppb and $\gamma^*\varphi$=0.0037) (McNamara et al., 2020), the simulated N_2O_5 mole ratio is 150 ppt (Fig. 6). In comparison, the minimum, average, and maximum N_2O_5 mole ratios observed from 04:00-08:00 EST on the clear case study night were 191 ppt, 229 ppt, and 274 ppt, respectively. As shown in Fig. S15, the mean observations of N_2O_5 from 04:00-08:00 EST were simulated by the model to occur at NO_2=9.1 ppb and $\gamma^*\varphi=10^{-2}$ (e.g. γ=0.01 and φ=1), and NO_2=1.9 ppb and $\gamma^*\varphi=10^{-4}$ (e.g. γ=0.001 and φ=0.1), which are plausible. However, the box model may be missing an N_2O_5 source due to the possible underprediction of N_2O_5 mole ratios during the clear case.

For the fog case study model results, the observed minimum, average, and maximum N_2O_5 mole ratios from 04:00-08:00 EST (1.2 ppt, 1.9 ppt, and 2.7 ppt, respectively,, Fig. 6) were not simulated to occur within reasonable model inputs (i.e. off-scale in Fig. S15). Considering the median $[NO_2]$ = 31 ppb and a $\gamma^*\varphi$ product of 0.0037 during Feb. 2016 in Ann Arbor, MI (McNamara et al., 2020), the model predicts 135 ppt of N_2O_5. Yet, even at 100 ppt of NO_2 (unrealistically low) and $\gamma^*\varphi=10^{-2}$ (e.g. γ=0.01 and φ=1), 3.4 ppt of N_2O_5 is simulated. This shows that the wide range of possible model conditions still overpredicts N_2O_5 abundance. Since NO_2 was likely >100 ppt in abundance, γ was likely <0.01, and φ

was likely <1 (*Sect. S1*), this supports fog droplet scavenging as a missing N_2O_5 sink (i.e. scavenging) earlier in the night. Yet, the maximum observed N_2O_5 mole ratio from 04:00 – 08:00 EST of the fog case night was 2.7 ppt (Fig. 6).

For the rainfall case study, the wide range of possible model conditions still overpredicts N_2O_5 abundance, similar to the fog case night. At a $\gamma^*\varphi$ product of 0.0037 (McNamara et al., 2020), an unrealistically low NO_2 mole ratio (~100 ppt) would be required (Fig. S15) to reach the average N_2O_5 mole ratio of 9.5 ppt observed between 04:00 and 08:00 EST on the rainfall case night (Fig. 6). Since NO_2 was likely >100 ppt in abundance, a missing sink (scavenging/wet deposition) of N_2O_5 is likely during the rainfall case. Considering the median $[NO_2]$ = 31 ppb and a $\gamma^*\varphi$ product of 0.0037 from our previous wintertime Ann Arbor, MI study (McNamara et al., 2020) results in 380 ppt of N_2O_5 simulated (Fig. 6). Yet, the maximum observed N_2O_5 mole ratio from 04:00 – 08:00 EST of the rainfall case night was 11.4 ppt (Fig. 6).

N_2O_5 abundance during the snowfall case was also overpredicted by the model, again implying a missing sink (scavenging/wet deposition). At a $\gamma^*\varphi$ product of 0.0037 (*Sect. S1*), an unrealistically low NO_2 mole ratio (~630 ppt) would be required (Fig. S15) to reach the average observation of N_2O_5 from the last 4 h of the snowfall case. Applying the median $[NO_2]$ = 31 ppb and a $\gamma^*\varphi$ product of 0.0037 from the previous wintertime Ann Arbor, MI study (McNamara et al., 2020) leads to 190 ppt of N_2O_5 based on these simulations. However, the maximum observed from 04:00-08:00 EST of the snowfall case was 34.2 ppt.

For the clear case study model results shown in Fig. S16, the mean $ClNO_2$ mole ratio from 04:00-08:00 EST (39.0 ppt) was simulated for NO_2=270 ppt and $\gamma^*\varphi=10^{-2}$ (e.g. γ=0.01 and φ=1) and NO_2=9.1 ppb and $\gamma^*\varphi=10^{-4}$ (e.g. γ=0.001 and φ=0.1), the latter of which corresponds to realistic values. At NO_2 and $\gamma^*\varphi$ levels corresponding to Feb. 2016 in Ann Arbor, MI (NO_2=31 ppb and $\gamma^*\varphi$=0.0037) (McNamara et al., 2020), the simulated $ClNO_2$ mole ratio was 280 ppt. However, the minimum, average, and maximum $ClNO_2$ mole ratios observed from 04:00-08:00 EST were 35.8 ppt, 39.0 ppt, and 45.2 ppt, respectively (Fig. 6). Notably, the box model overpredicted $ClNO_2$ mole ratios during the clear case for the prior Ann Arbor conditions, despite having underpredicted N_2O_5 mole ratios under the same conditions. This points to the variability and need to better constrain $\gamma^*\varphi$ (N_2O_5 uptake and $ClNO_2$ yield).

The maximum observed $ClNO_2$ mole ratio from the last 4 h of the fog case study (04:00 – 08:00 EST) was 2.5 ppt. Applying the median $[NO_2]$ = 31 ppb and a $\gamma^*\varphi$ product of 0.0037 from Ann Arbor, MI during Feb. 2016 (McNamara et al., 2020) results in 140 ppt of $ClNO_2$ being simulated (Fig. 6). At a $\gamma^*\varphi$ product of 0.0037, an unrealistically low value of 100 ppt of NO_2 would still produce 7.3 ppt of $ClNO_2$ (Fig. S16). A $\gamma^*\varphi$ product of $<10^{-3}$ (0.001) and $[NO_2]$ = 100 ppt would be required to match the average observation of $ClNO_2$ (2.1 ppt) from 04:00 – 08:00 EST. However, NO_2 was likely >100 ppt in abundance, and the $\gamma^*\varphi$ product was likely $\geq 10^{-3}$. This overprediction of $ClNO_2$ mole ratios, by ~50 times, was similar to the overprediction of N_2O_5 mole ratios, further supporting fog droplet N_2O_5 scavenging, not represented by the model, as the reason for the $ClNO_2$ overprediction.

The maximum observed $ClNO_2$ mole ratio from the last 4 h of the rainfall case study (04:00 – 08:00 EST) was 3.2 ppt. Applying the median $[NO_2]$ = 31 ppb and a $\gamma^*\varphi$ product of 0.0037 from Ann Arbor, MI during Feb. 2016 (McNamara et al., 2020) results in the simulation of 280 ppt of $ClNO_2$ (Fig. 6). At a $\gamma^*\varphi$ product of 0.0037, an unrealistically low value of 100 ppt of NO_2 would still produce 5.0 ppt of $ClNO_2$(Fig. S16). Since NO_2 was likely >100 ppt in abundance, this suggests a missing sink (scavenging) for the rainfall case, similar to the fog droplet case. This overprediction of $ClNO_2$ mole ratios (by ~90 times) was larger than the overprediction of N_2O_5 mole ratios (by ~30 times) during the rainfall case, suggesting that $ClNO_2$, in addition to N_2O_5, is scavenged by the rain droplets.

For the snowfall case, applying the median $[NO_2]$ = 31 ppb and a $\gamma^*\varphi$ product of 0.0037 from Ann Arbor, MI during Feb. 2016 (McNamara et al., 2020) results in 400 ppt of $ClNO_2$ being simulated. However, the maximum observed $ClNO_2$ mole ratio during the final 4 h of the snowfall case (04:00 – 08:00 EST) was 33.6 ppt. The box model overpredicted $ClNO_2$ mole ratios during the snowfall case (by ~12 times, as compared to ~5 times for N_2O_5 mole ratios). At a $\gamma^*\varphi$ product of 0.0037 (*Sect. S1*), a low mole ratio of ~200 ppt of NO_2 would be required to reach the average observation of $ClNO_2$ from the last 4 h of the snowfall case (27.2 ppt), suggesting a missing sink (scavenging) affecting both N_2O_5 and $ClNO_2$ abundance during the snowfall case.

165

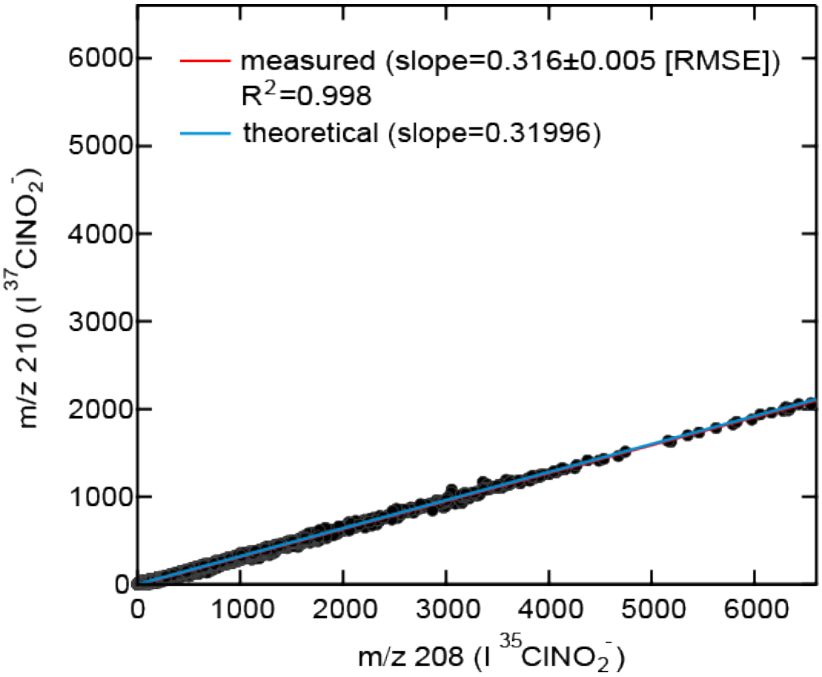

Figure S1: Plot of 5-min averaged, background subtracted, signals for m/z 210 vs. m/z 208, showing the isotopic ratio used to identify $ClNO_2$.

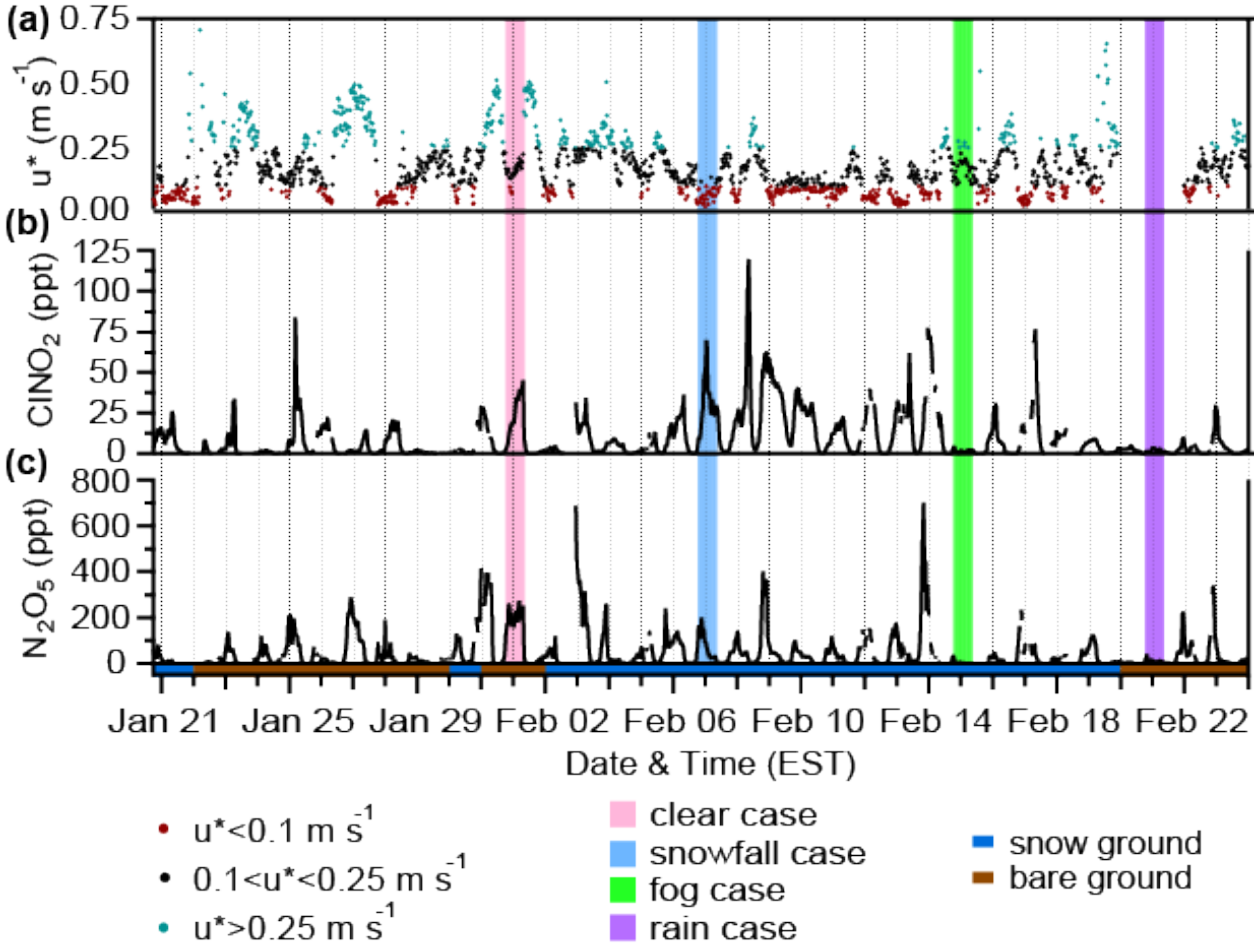

Figure S2: 30 min averaged (a) friction velocities (u*, m s^{-1}) and (b) $ClNO_2$ and (c) N_2O_5 mole ratios from January 20 to February 24, 2018. Friction velocities are divided into three categories: lower (u*<0.1 m s^{-1}, red), intermediate (0.1<u*<0.25 m s^{-1}, black), and higher (u*>0.25 m s^{-1}, aqua). The shading below the x-axis represents ground cover – snow (blue) or bare ground (brown). Vertical shading represents the example case studies: clear (pink), snowfall (light blue), fog (green), and rain (purple). Gaps in the $ClNO_2$ and N_2O_5 timeseries are due to experiments described by (McNamara et al., 2021).

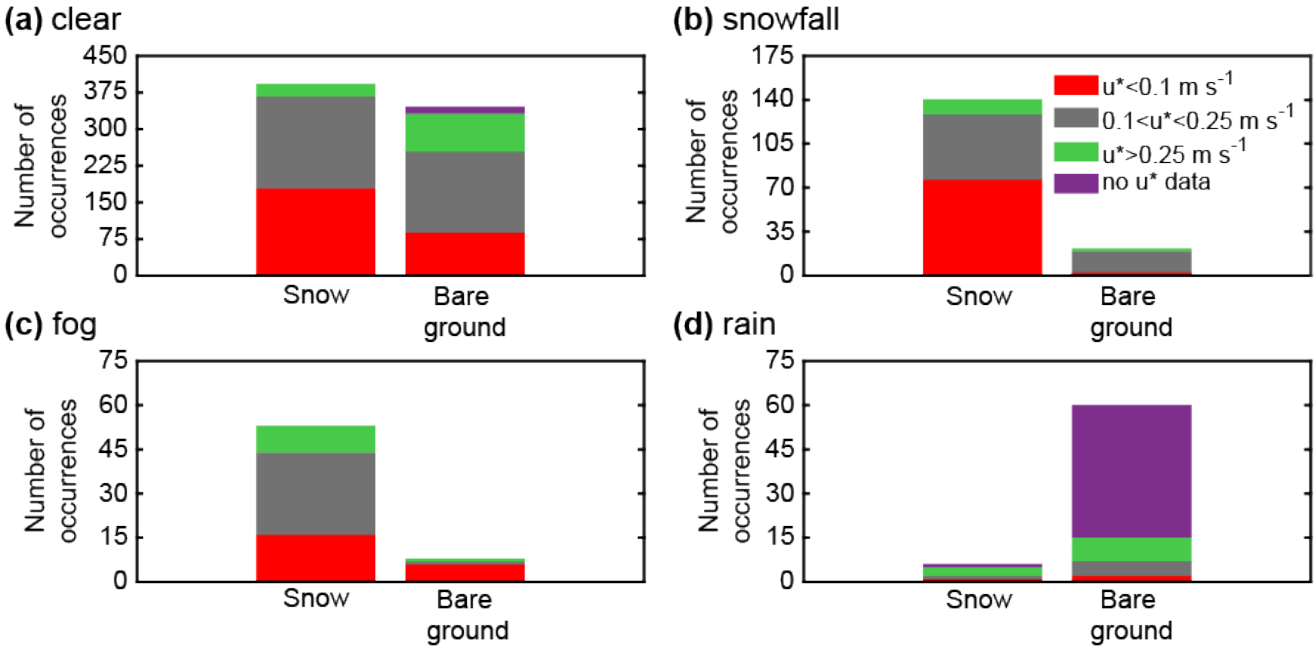

Figure S3: Stacked bar graphs showing the number of occurrences between 18:00 and 08:00 (30 min time resolution) of lower- ($u^*<0.1$ m s^{-1}), mid- ($0.1<u^*<0.25$ m s^{-1}), and higher-turbulence ($u^*>0.25$ m s^{-1}) over snow-covered and bare ground, during (a) clear, (b) snowfall, (c) fog, and (d) rainfall conditions. Lower turbulence occurred 39% of the time, mid-turbulence occurred 42% of the time, and higher turbulence occurred 14% of the time. Snowfall and fog both primarily occurred over snow-covered ground (87% of the time). Rainfall occurred over bare ground 92% of the time. Clear conditions had snow-covered and bare ground 58% and 42% of the time, respectively. Lower-turbulence accompanied snow-covered ground 71% of the time, and higher-turbulence accompanied bare ground 64% of the time. The most frequent turbulence bin to occur during snowfall and fog was $u_*<0.1$ m s^{-1}, representing 59% and 55% of the occurrences during these periods, respectively. Clear conditions had $0.1<u_*<0.25$ m s^{-1} as the most frequent bin, followed by $u_*<0.1$ m s^{-1}, representing 48% and 36% of these periods, respectively. In contrast, the most frequent turbulence bin to occur during rainfall was $u_*>0.25$ m s^{-1}, representing 17% of all occurrences during rain and 55% of the periods for which measurements were available. Sonic anemometer measurements, and therefore calculated u_* values, are unavailable from February 20-21.

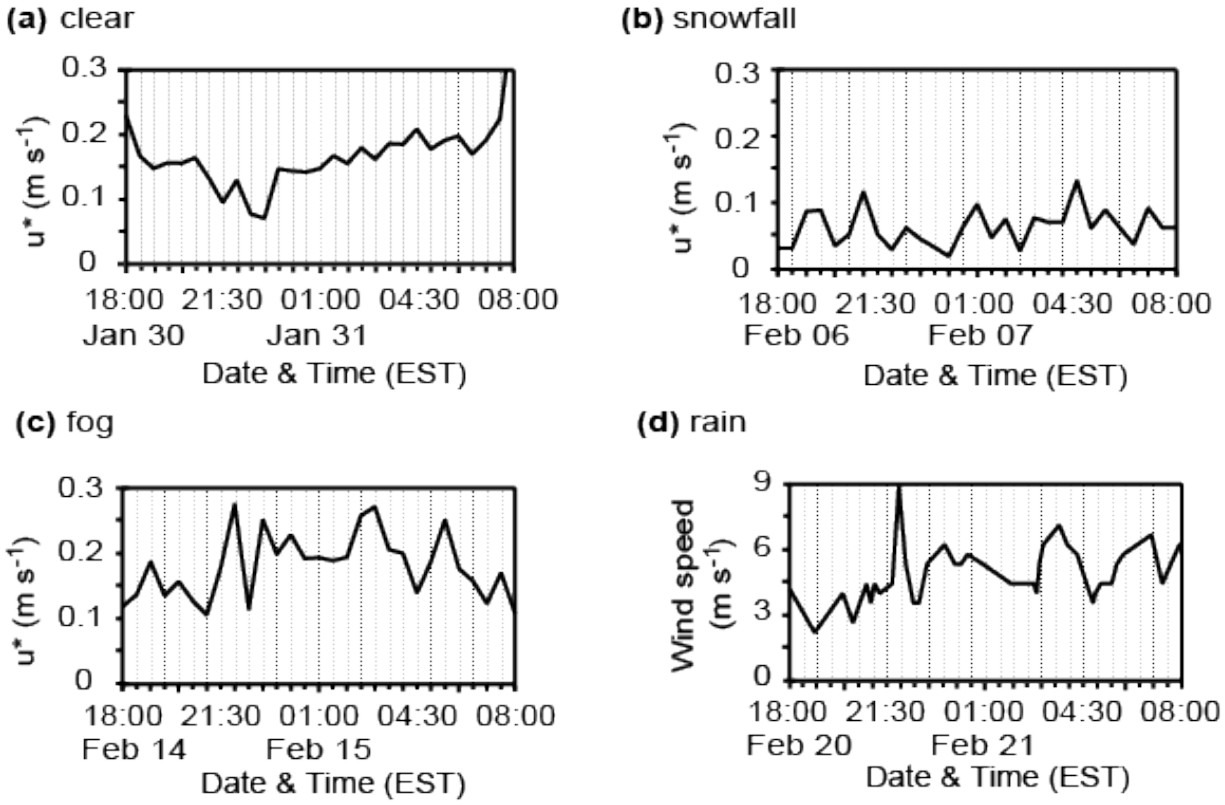

Figure S4: Friction velocity or wind speed between 18:00 and 08:00 h EST for each of the case studies presented – (a) clear, (b) snowfall, (c) fog, and (d) rainfall. Friction velocity could not be calculated for the rainfall case because sonic anemometer data were unavailable. Wind speed is substituted, and the relationship between wind speed and friction velocity is described in Figure S5.

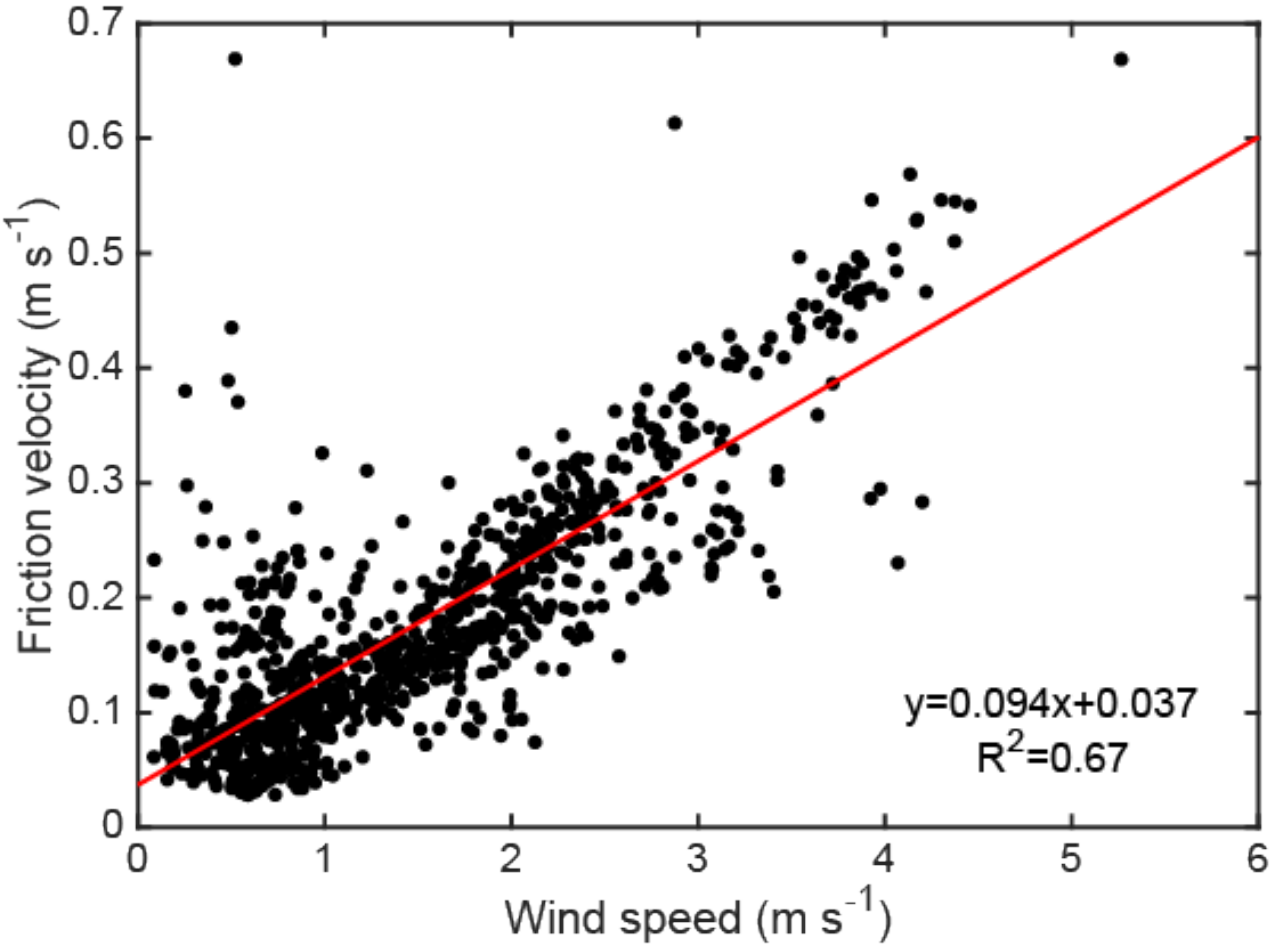

200 **Figure S5:** Relationship between friction velocity and wind speed, measured by the sonic anemometer at 20 Hz and plotted as 30-min averages. This linear regression indicates that for wind speed values greater than 2.3 m s^{-1}, the friction velocity was above 0.25 m s^{-1} (consistent with higher turbulence in the context of this study).

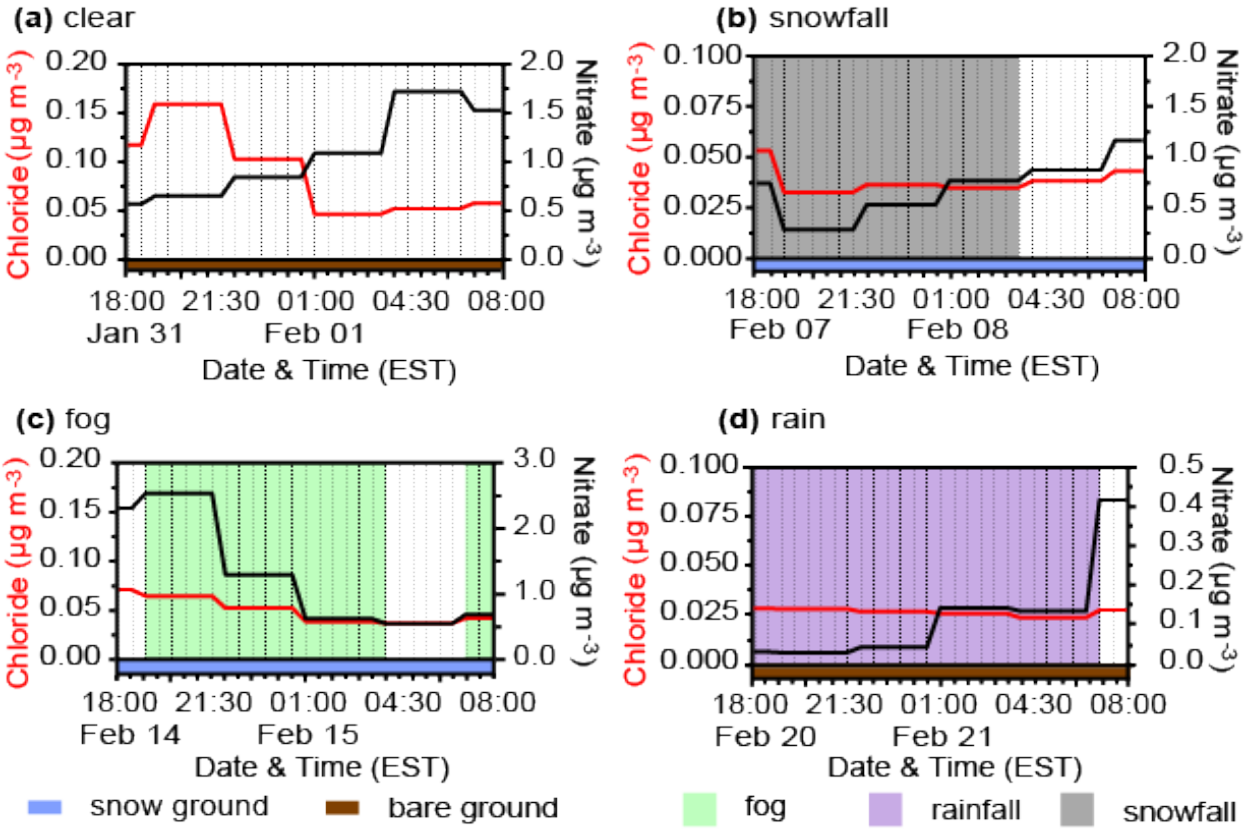

Figure S6: $PM_{2.5}$ chloride and nitrate concentrations between 18:00 and 08:00 h EST for each of the case studies presented – (a) clear air, (b) snowfall, (c) fog, and (d) rainfall. AIM-IC data were unavailable for the snowfall case night of February 06-07; therefore, we instead show a similar night, February 07-08 (the night after the snowfall case study) for comparison. The snowfall case study night and its substitution were similar in respect to snowfall and ground cover, but the substituted night had a higher friction velocity (average $u^* = 0.12$ m s^{-1}, whereas the snowfall case had an average $u^* = 0.06$ m s^{-1}).

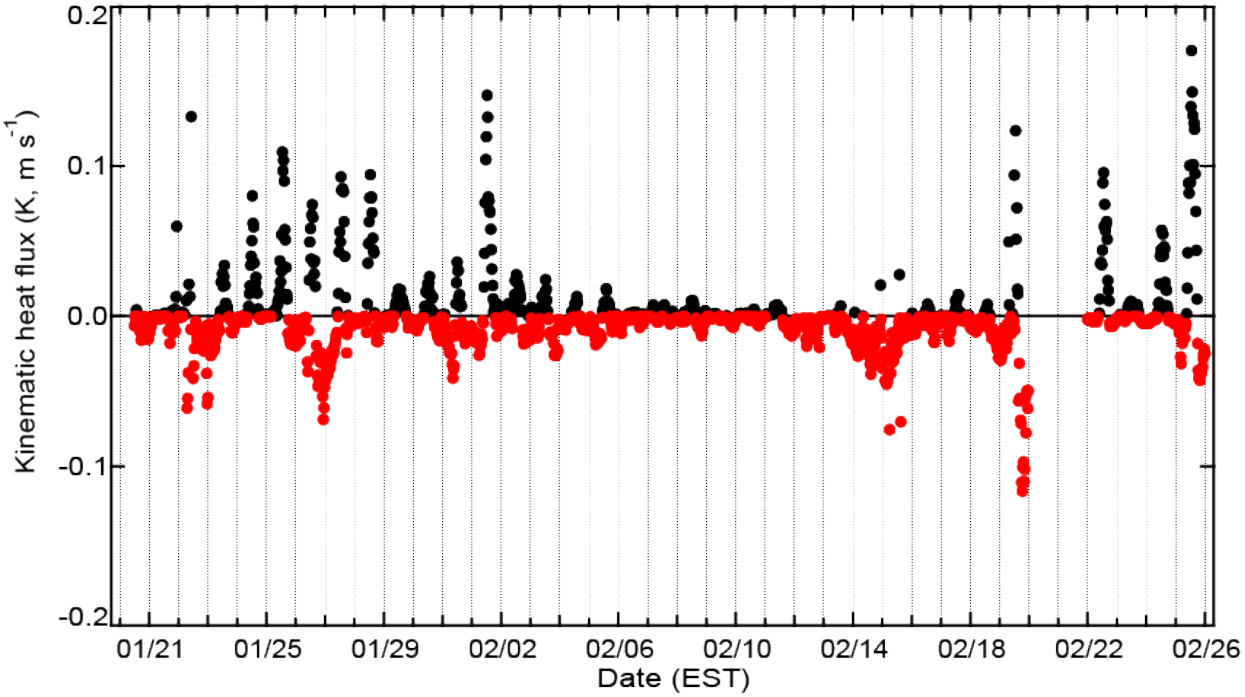

Figure S7: Temporal variation of 30 min averaged kinematic heat flux throughout the duration of the study. Values less than zero, indicating a temperature inversion, are shown in red. A temperature inversion occurred during every night for which sonic anemometer data was available. Data sets were unavailable from 20 to 21 February due to complications associated with heavy rainfall.

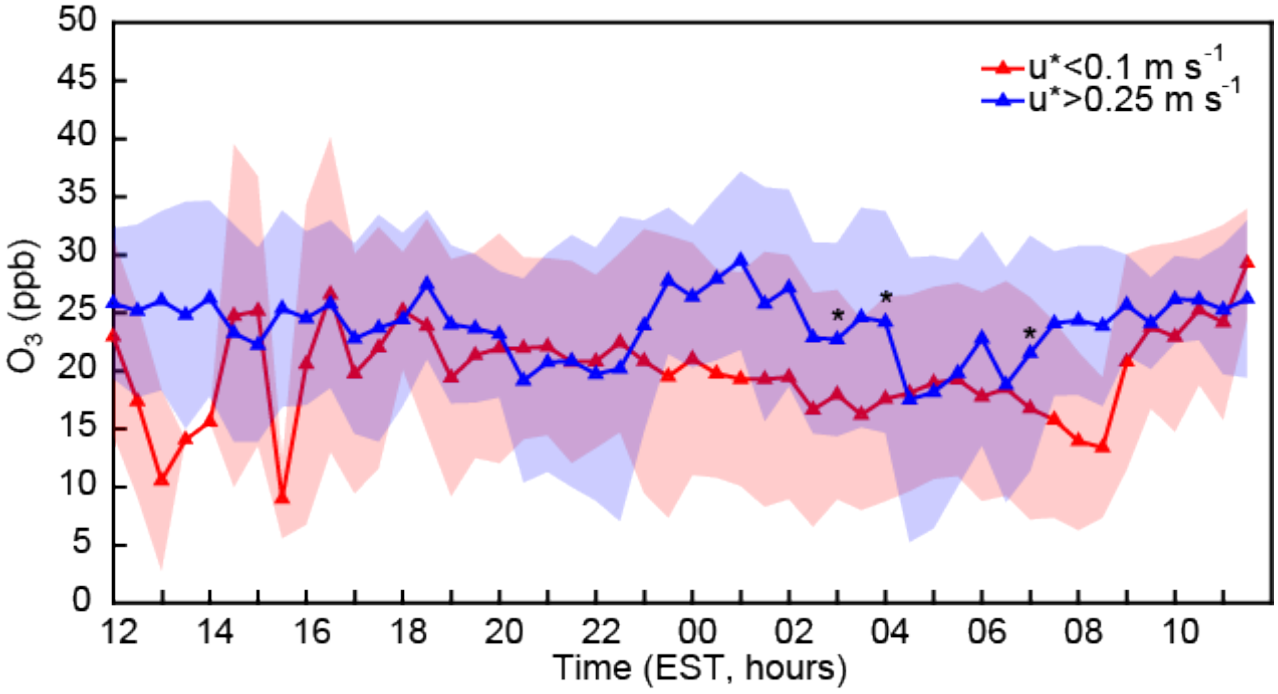

Figure S8: Diel patterns of 30 min averaged mole ratios of ozone (O_3) binned by lower ($u^* < 0.1$ m s^{-1}) and higher ($u^* > 0.25$ m s^{-1}) turbulence conditions from January 20 - February 24. Shading represents one standard deviation. Asterisks represent statistically significant (t-test) differences at the $p<0.05$ level between lower and higher turbulence conditions for each 30 min time period. Considering the statistically
225 significantly different periods of 03:00, 04:30, and 07:00 h, ozone mole ratios are 7.0 ppb (1.4-fold) higher during higher-turbulence, conditions, on average. For the entire nighttime period (18:00-08:00 h), much of which is not statistically significantly different between the two turbulence bins, ozone mole ratios were 3.2 ppb (1.2-fold) higher during higher-turbulence conditions, on average.

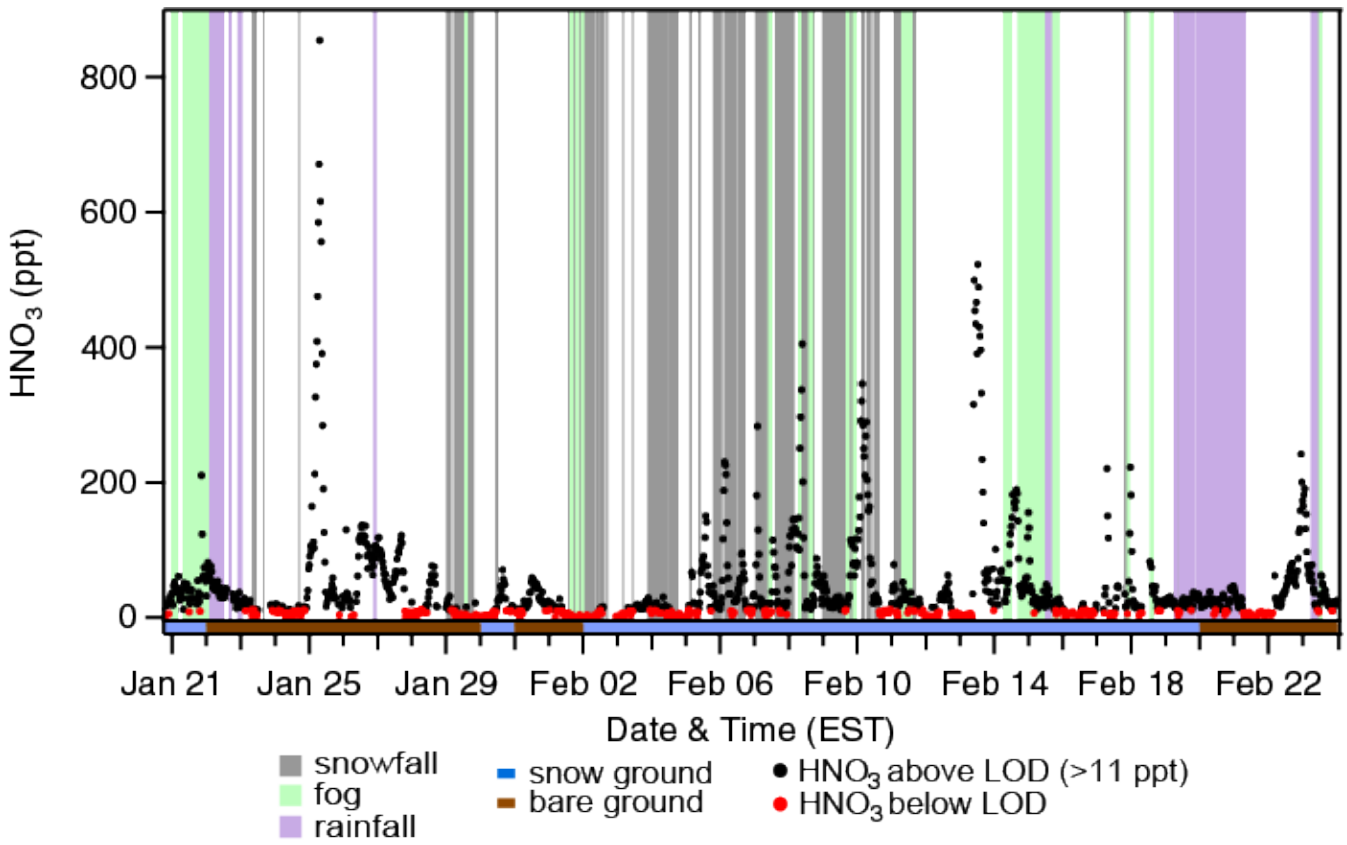

Figure S9: Mole ratios of 30 min averaged HNO_3 during the campaign, and occurrence of snowfall (gray), fog (green), and rainfall (purple). The shading below the x-axis represents ground cover – snow (blue) or bare ground (brown). Considering periods between 18:00 and 08:00 EST when HNO_3 was above LOD, where n=number of 30 min periods, the air was clear 63% of the time [n=376], snowfall occurred 18% of the time [n=105], rainfall occurred 10% of the time [n=60], and fog occurred 9% of the time [n=52]. The total number of 30 min periods for which HNO_3 was above LOD during nighttime was 593, or 60% of the nighttime data during the campaign. These data represent lower limits as they were not adjusted for the poor background scrubbing efficiency of 12±1%, and therefore, should only be viewed qualitatively.

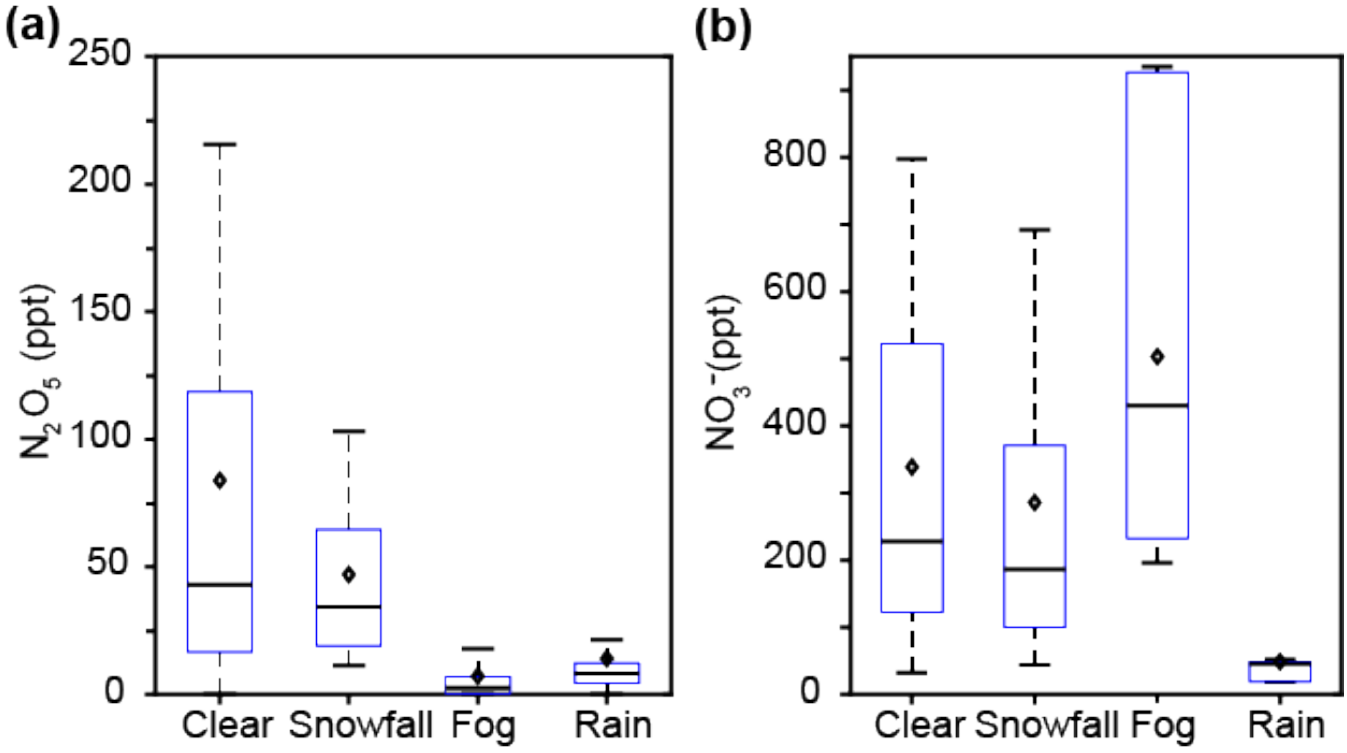

Figure S10: Box plots showing 30 min averaged mole ratios of (a) N_2O_5 and (b) $PM_{2.5}$ NO_3^- during clear conditions and weather events (snowfall, fog, and rain) from January 20-February 24. Bars represent the 10th, 50th, and 90th percentiles, boxes represent the 25th and 75th percentiles, and diamonds represent the means. Only nighttime data between 18:00 and 08:00 h EST are included. The purpose of this figure is to show how the decrease in N_2O_5 compares to the increase in NO_3^- during fog in units that are appropriate for direct comparison. During fog, N_2O_5 mole ratios were lower by 77±5 ppt, and $PM_{2.5}$ NO_3^- mole ratios were higher by 160±20 ppt, in comparison to clear conditions.

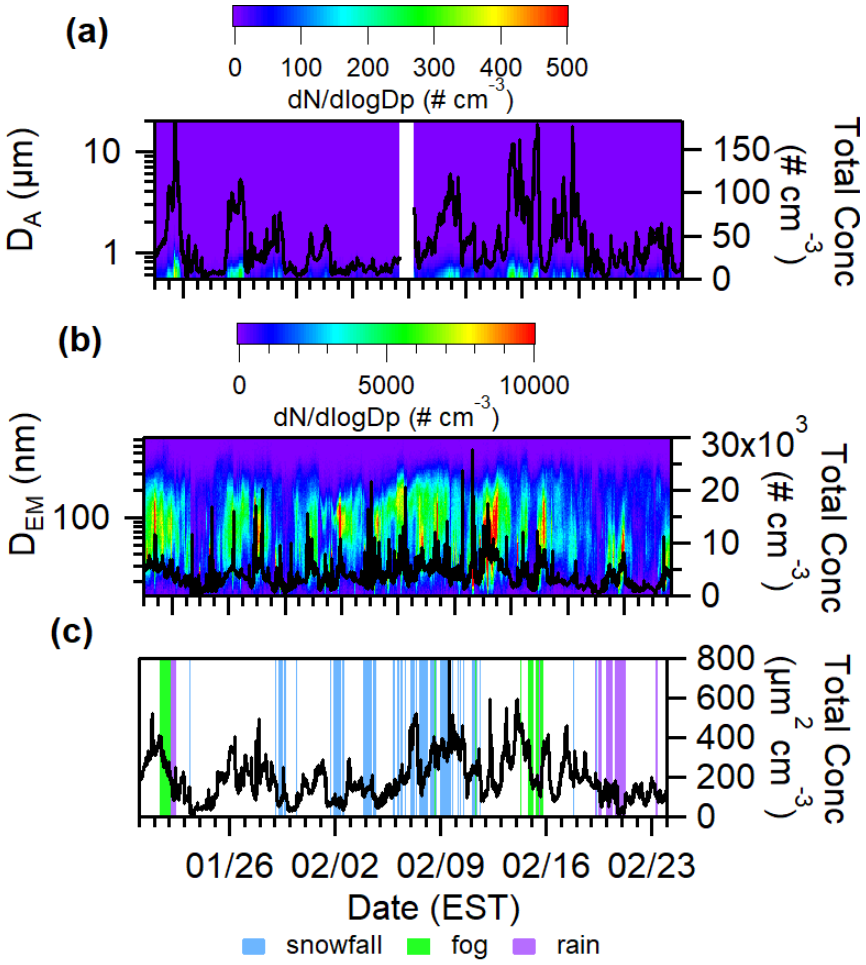

Figure S11: Temporal variations in (a) aerosol size distributions and total number concentrations from the aerodynamic particle sizer (APS, model 3321, TSI, Inc.), which measured aerodynamic diameter (D_A) from 0.5-20 µm, (b) aerosol size distributions and total number concentrations from the scanning mobility particle sizer (SMPS, model 3082, TSI, Inc.), which measured electrical mobility diameter (D_{EM}) from 14.1-736.5 nm, and (c) total (D_{EM} 14.1-736.5 nm) surface area concentrations measured by the SMPS, where shading represents the occurrence of snowfall (light blue), fog (green), and rainfall (purple).

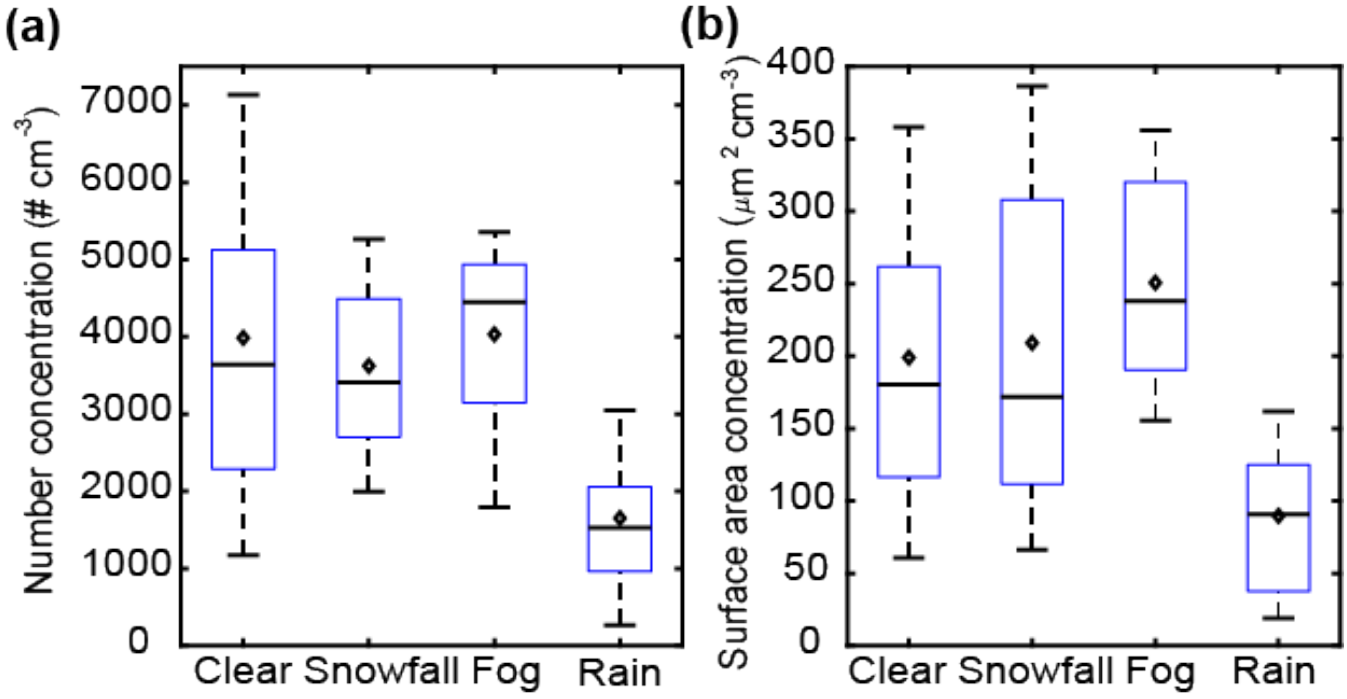

Figure S12: Box plots showing 30 min averaged submicron (D_{EM} 14.1-736.5 nm)) (a) number and (b) surface area concentrations during nighttime (18:00 – 08:00 EST) clear conditions and weather events (snowfall, fog, and rain) from January 20-February 24. Bars represent the 10th, 50th, and 90th percentiles, boxes represent the 25th and 75th percentiles, and diamonds represent the means. Number concentrations are not statistically significantly different between clear and snowfall conditions (p=0.06), clear and fog conditions (p=0.88), or between snowfall and fog conditions (p=0.06). Surface area concentrations are not statistically significantly different between clear and snowfall conditions (p=0.32). The remaining comparisons between aerosol concentrations across the weather conditions are statistically significant (p<0.05). Number concentrations were 2300±120 particles cm^{-3} (2.4 times) lower during rainfall in comparison to clear conditions. Surface area concentrations were 109±6 μm^2 cm^{-3} (2.2 times) lower during rainfall, and 52±7 μm^2 cm^{-3} (1.3 times) higher during fog, in comparison to clear conditions.

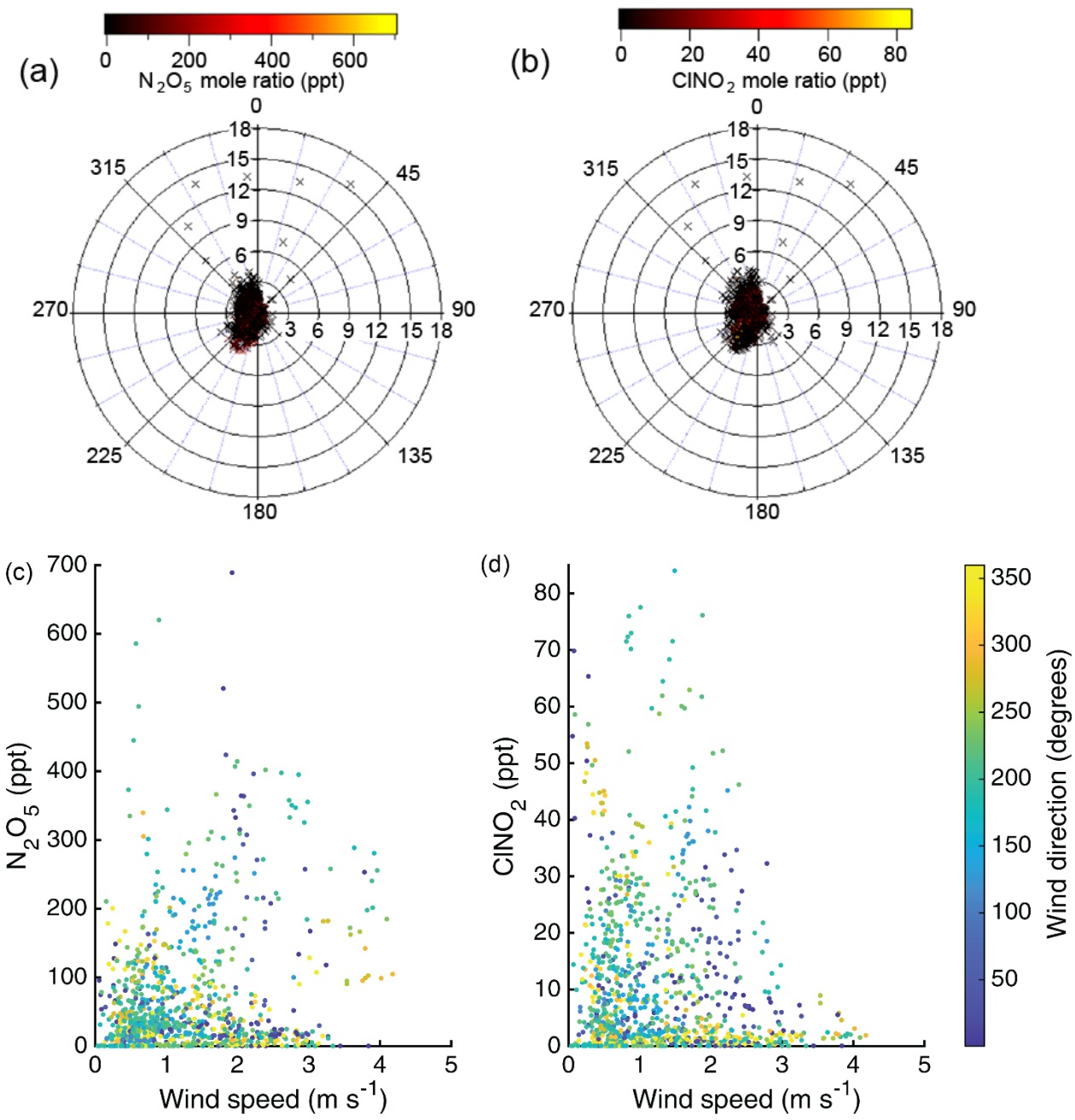

Figure S13: Polar plots show 30 min averaged wind direction (angle, degrees), 30 min averaged wind speed (radius, m s^{-1}), and 30 min averaged N_2O_5 mole ratios (a) and $ClNO_2$ mole ratios (b) on a colorscale. Plots of nighttime N_2O_5 mole ratios vs wind speed (c) and nighttime $ClNO_2$ mole ratios vs wind speed (d), with wind direction shown as a colorscale. No clear correlation is observed between wind speed or direction and N_2O_5 or $ClNO_2$ abundance.

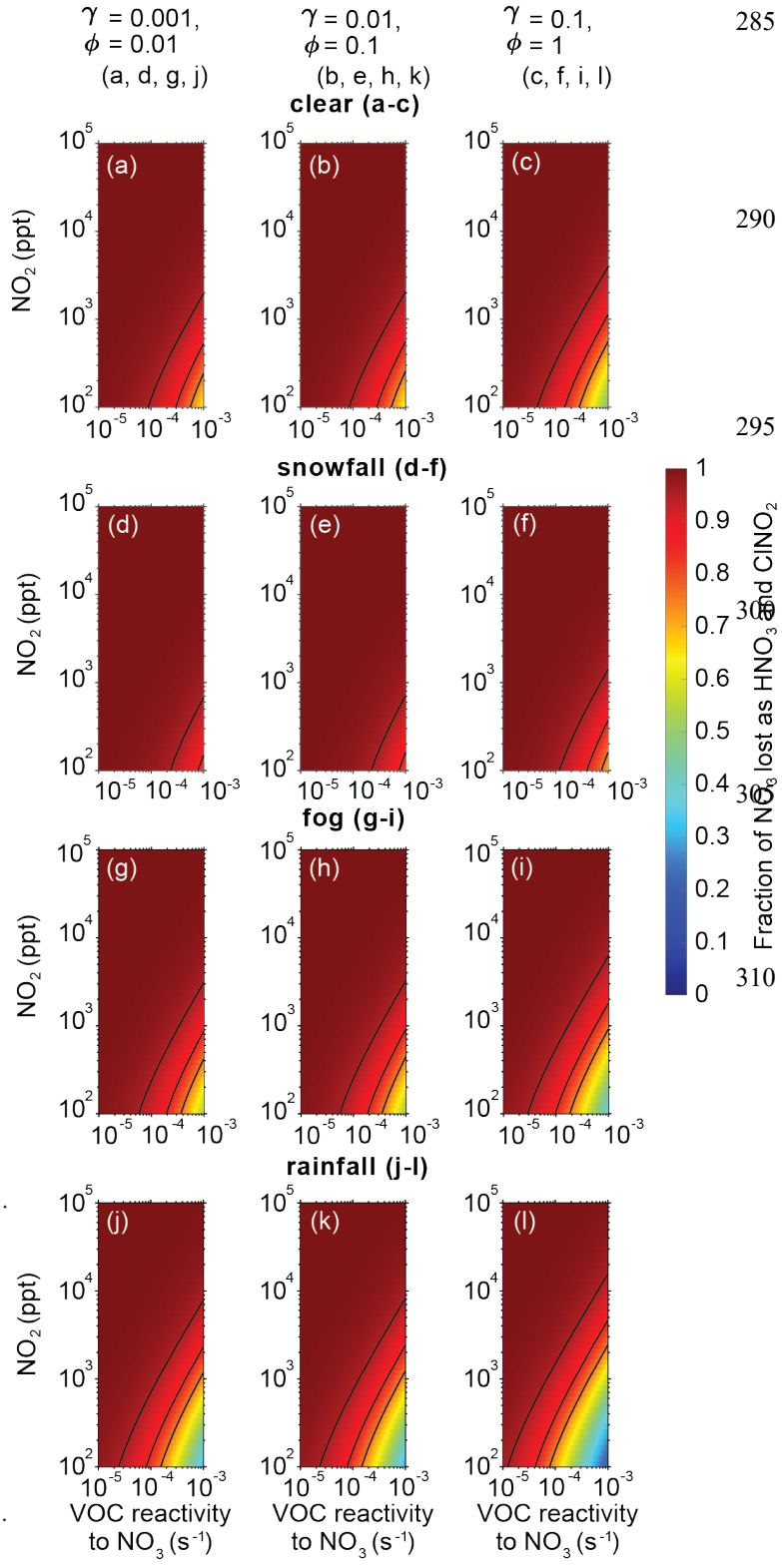

Figure S14: Fraction of NO_3 lost to inorganic pathways (i.e. through production of HNO_3 and $ClNO_2$, compared to reaction with VOCs), $\frac{P(HNO_3)+P(ClNO_2)}{P(HNO_3)+P(ClNO_2)+P(NO_3+VOC)}$, where $P(HNO_3)$ = HNO_3 production (R-S6), $P(ClNO_2)$ = $ClNO_2$ production (R-S7), and $P(NO_3+VOC)$ = reaction of NO_3 with VOCs (R-S4), plotted as a function of NO_2 mole ratio (ppt) and VOC reactivity to NO_3 (s^{-1}) for three different combinations of γ and φ (γ=0.001 and φ=0.01 [a, d, g, j], γ=0.01 and φ=0.1 [b, e, h, k], and γ=0.1 and φ=1 [c, f, i, l]). Black contour lines correspond to 75%, 85%, and 95% of NO_3 lost through inorganic pathways. When only two contours are shown, this corresponds to the 75th percentile off-scale, with only the 85th and 95th percentiles shown. Each set of three panels corresponds to each of the four case study nights: Jan 31-Feb 1 - clear (a-c), Feb 6-7 - snowfall (d-f), Feb 14-15 - fog (g-i), and Feb 20-21 - rainfall (j-l).

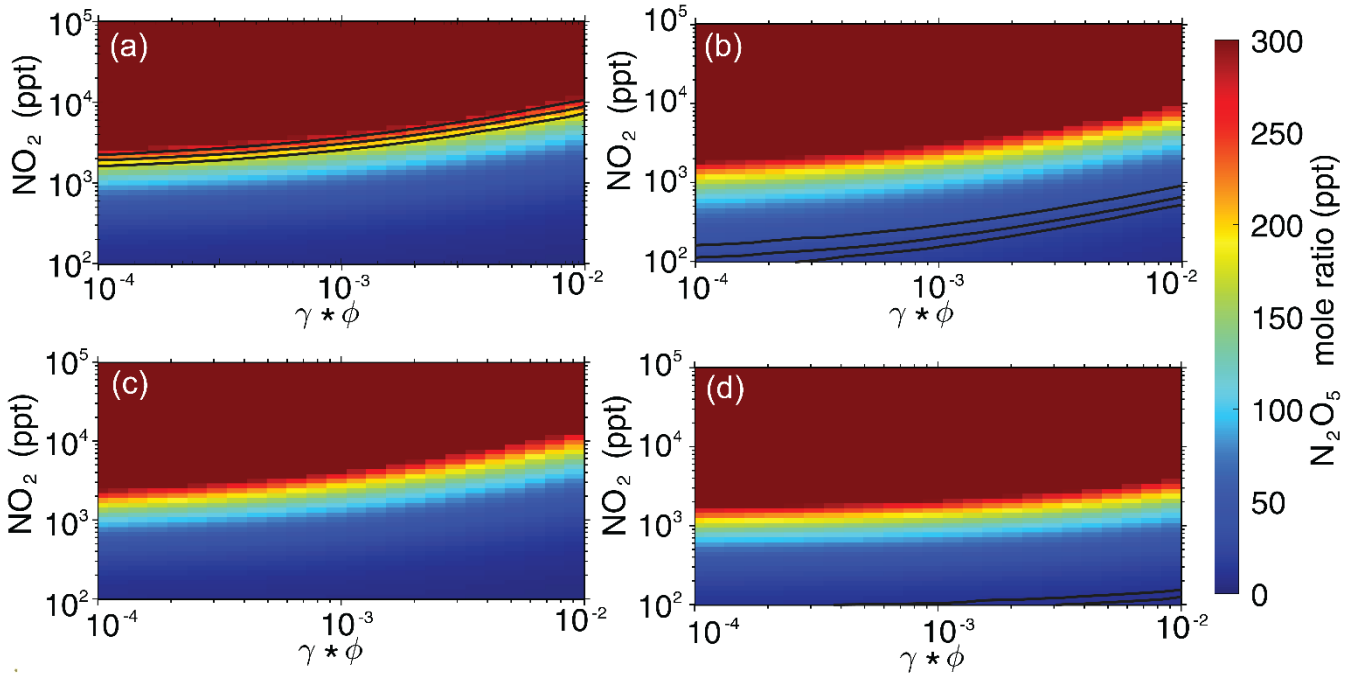

Figure S15: Simulated average N_2O_5 mole ratios from the final 4 h (corresponding to 04:00-08:00 EST) of a 14 h model run as a function of NO_2 mole ratio (ppt) and γ*φ products (N_2O_5 uptake * $ClNO_2$ yield) for the four case nights: Jan 31-Feb 1 - clear (a), Feb 6-7 - snowfall (b), Feb 14-15 - fog (c), and Feb 20-21 - rainfall (d). Contours represent the minimum, average, and maximum N_2O_5 mole ratios observed during the final 4 h of each case study period, with these values being offscale for the fog (c) and rainfall (d) cases, as discussed in Section S2. For these simulations, the reactivity of VOCs to NO_3 was held constant at 10^{-4} s^{-1}.

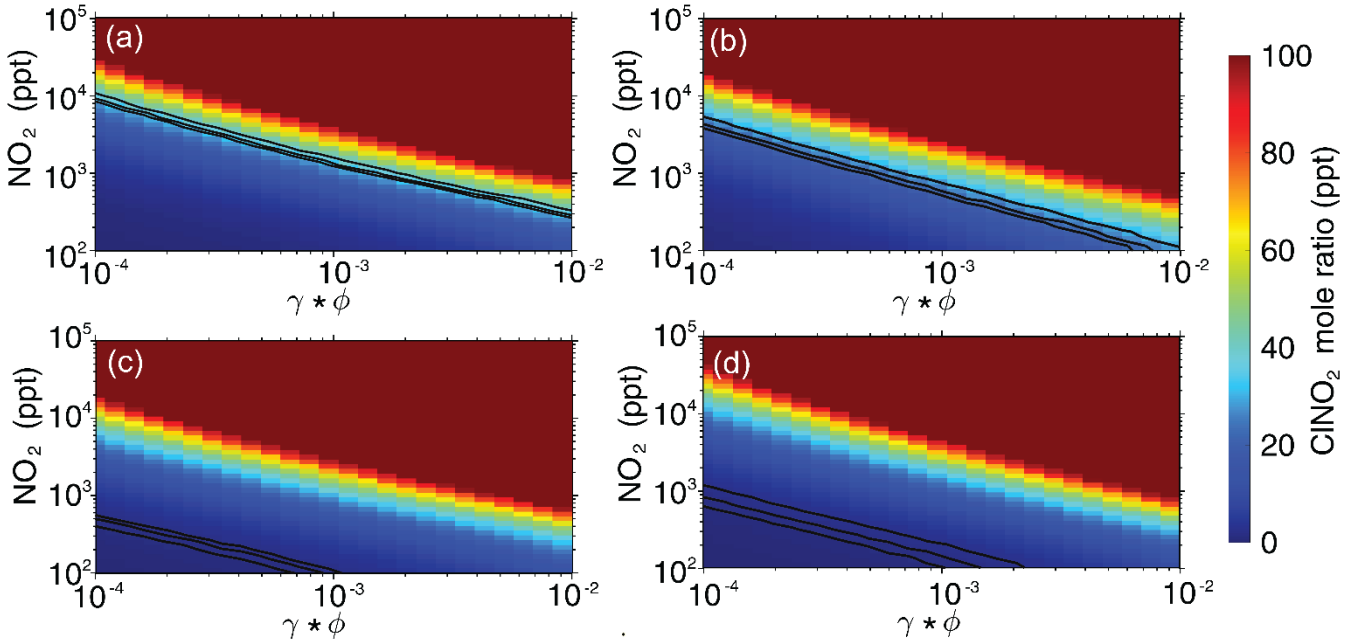

Figure S16: Simulated average $ClNO_2$ mole ratios from the final 4 h of a 14 h model run (meant to simulate the 18:00-08:00 nighttime period) as a function of NO_2 concentration (ppt) and γ*φ products for the four case nights, Jan 31-Feb 1 - clear (a), Feb 6-7 - snowfall (b), Feb 14-15 - fog (c), and rainfall (d). Contours represent the minimum, average, and maximum $ClNO_2$ mole ratios observed during the final 4 h of each case study period. For these simulations, the reactivity of VOCs to NO_3 was held constant at 10^{-4} s^{-1}, as we determined previously (Fig S13) that the VOC loss pathway for NO_3 is minor in this wintertime MI environment.

Table S1: Ranges, medians, averages, and 95% confidence intervals for mole ratios of $ClNO_2$ and N_2O_5, $PM_{2.5}$ concentrations of Cl^- and NO_3^-, temperature, relative humidity (RH), and friction velocity (u*) measured across the entire campaign, between 18:00-08:00 EST. Data below the limit of detection (LOD) were applied as $\frac{1}{2}$×LOD in calculations.

	Clear	Snowfall	Fog	Rain
$ClNO_2$ range (ppt)	0.05-84	0.05-70	0.05-76	0.05-5.25
$ClNO_2$ median (ppt)	6.3	11.9	1.0	2.59
$ClNO_2$ average ± 95% confidence interval (ppt)	11.8±0.7	16.8±0.7	5.0±0.6	2.27±0.06
N_2O_5 range (ppt)	0.15-702	0.15-257	0.15-55	0.15-289
N_2O_5 median (ppt)	43	34	2.4	8
N_2O_5 average ± 95% confidence interval (ppt)	84±5	47±2	7.1±0.6	14±2
Cl^- range (μg m^{-3})	0.040-0.910	0.040-0.645	0.197-0.717	0.03-0.57
Cl^- median (μg m^{-3})	0.228	0.213	0.374	0.12
Cl^- average ± 95% confidence interval (μg m^{-3})	0.257±0.007	0.258±0.006	0.456±0.008	0.22±0.01
NO_3^- range (μg m^{-3})	0.03-3.9	0.07-2.50	0.11-3.9	0.027-0.707
NO_3^- median (μg m^{-3})	0.64	0.53	1.17	0.118
NO_3^- average ± 95% confidence interval (μg m^{-3})	0.95±0.04	0.81±0.03	1.38±0.04	0.126±0.007
Temperature range (K)	258.5-288.7	260.3-271.9	260.6-282.8	273.2-288.8
Temperature median (K)	271.2	264.9	277.3	283.3
Temperature average ± 95% confidence interval (K)	270.8±0.3	265.8±0.2	276.7±0.2	282.1±0.2
RH range (%)	39-97	64-97	73-100	39-97
RH median (%)	76.0	84.0	96.0	92.5
RH average ± 95% confidence interval (%)	75.0±0.5	82.9±0.3	93.7±0.3	90.2±0.4
u* range (m s^{-1})	0.032-0.498	0.027-0.509	0.029-0.719	0.03-0.74
u* median (m s^{-1})	0.133	0.102	0.123	0.30
u* average ± 95% confidence interval (m s^{-1})	0.150±0.004	0.129±0.004	0.162±0.007	0.36±0.01

Table S2: Ranges, medians, averages, and 95% confidence intervals for mole ratios of $ClNO_2$ and N_2O_5, $PM_{2.5}$ concentrations of Cl^- and NO_3^-, temperature, relative humidity (RH), and friction velocity (u*) observed during each of the case study periods, between 18:00-08:00 EST. Data below the limit of detection (LOD) were applied as $\frac{1}{2}$×LOD in calculations.

	Clear (Jan 31-Feb 01)	Snowfall (Feb 06-07)	Fog (Feb 14-15)	Rain (Feb 20-21)
$ClNO_2$ range (ppt)	1.5-45	2.4-70	0.6-4.5	0.6-3.7
$ClNO_2$ median (ppt)	21	28	1.6	1.8
$ClNO_2$ average ± 95% confidence interval (ppt)	23±5	30±6	1.8±0.4	2.0±0.3
N_2O_5 range (ppt)	75-274	22-201	1.1-31	7.1-40
N_2O_5 median (ppt)	207	71	2.7	11
N_2O_5 average ± 95% confidence interval (ppt)	200±16	82±21	5±3	13±4
Cl^- range (μg m^{-3})	0.05-0.16	0.033-0.043*	0.037-0.065	0.023-0.028
Cl^- median (μg m^{-3})	0.08	0.036*	0.042	0.026
Cl^- average ± 95% confidence interval (μg m^{-3})	0.09±0.04	0.037±0.004*	0.047±0.04	0.026±0.03
NO_3^- range (μg m^{-3})	0.7-1.7	0.3-1.2*	0.5-2.5	0.025-0.4
NO_3^- median (μg m^{-3})	1.1	0.7*	0.7	0.1
NO_3^- average ± 95% confidence interval (μg m^{-3})	1.2±0.4	0.7±0.3*	1.1±0.7	0.2±0.1
Temperature range (K)	273.1-276.6	263.7-266.1	276.0-282.8	273.2-287.6†
Temperature median (K)	274.6	265.0	280.1	278.2†
Temperature average ± 95% confidence interval (K)	274.8±0.4	265.1±0.3	279.7±0.9	279±2†
RH range (%)	62-76	63-88	92-100	85-93
RH median (%)	72	79	96	89
RH average ± 95% confidence interval (%)	72±1	78±3	96±1	89±1
u* range ($m\ s^{-1}$)	0.07-0.23	0.02-0.13	0.11-0.28	2.2-8.9 (0.25-0.46) †
u* median ($m\ s^{-1}$)	0.16	0.06	0.19	4.5 (0.46) †
u* average ± 95% confidence interval ($m\ s^{-1}$)	0.16±0.01	0.06±0.01	0.18±0.02	5.0±0.5 (0.50±0.08) †

* Because the AIM-IC was not operational during the snowfall case study, the following night (February 07-08) is substituted for concentrations of Cl^- and NO_3^-. The snowfall case study night and its substitution were similar in respect to snowfall and ground cover, but the substituted night had a higher friction velocity (average u*=0.12 $m\ s^{-1}$, whereas the snowfall case had an average u*=0.06 $m\ s^{-1}$).

† Because the sonic anemometer was not operational during the rainfall case, we use temperature and wind speed values from the Kalamazoo−Battle Creek International Airport (KAZO) located ~7 km to the southeast and retrieved from Weather Underground (https://www.wunderground.com/history/daily/us/mi/kalamazoo/KAZO). We provide estimated u* values in parentheses, calculated using the linear regression of u* vs wind speed in Figure S5.

Table S3: Mean aerosol surface area (14.1-736.5 nm), pressure, ozone mole ratios, and temperature for each case study night. These were were used as inputs for box modeling.

	Clear (Jan 31-Feb 01)	**Snowfall (Feb 06-07)**	**Fog (Feb 14-15)**	**Rain (Feb 20-21)**
Aerosol surface area (μm^2 cm^{-3})	199.0	209.1	250.7	89.8
Pressure (hPa)	975.3	995.6	978.1	988.8
Ozone (nmol mol^{-1}, ppb)	12.8	24.4	14.4	18.3
Temperature (K)	274.8	265.1	279.7	279.0

370

References

Bertram, T. H. and Thornton, J. A.: Toward a general parameterization of N_2O_5 reactivity on aqueous particles: the competing effects of particle liquid water, nitrate and chloride, Atmos. Chem. Phys., 9, 8351–8363, doi:10.5194/acp-9-8351-2009, 2009.

Kenagy, H. S., Sparks, T. L., Wooldridge, P. J., Weinheimer, A. J., Ryerson, T. B., Blake, D. R., Hornbrook, R. S., Apel, E. C. and Cohen, R. C.: Evidence of Nighttime Production of Organic Nitrates During SEAC4RS, FRAPPÉ, and KORUS-AQ, Geophys. Res. Lett., 47(11), 1–9, doi:10.1029/2020GL087860, 2020.

McDuffie, E. E., Fibiger, D. L., Dubé, W. P., Lopez Hilfiker, F., Lee, B. H., Jaeglé, L., Guo, H., Weber, R. J., Reeves, J. M., Weinheimer, A. J., Schroder, J. C., Campuzano-Jost, P., Jimenez, J. L., Dibb, J. E., Veres, P., Ebben, C., Sparks, T. L., Wooldridge, P. J., Cohen, R. C., Campos, T., Hall, S. R., Ullmann, K., Roberts, J. M., Thornton, J. A. and Brown, S. S.: $ClNO_2$ Yields From Aircraft Measurements During the 2015 WINTER Campaign and Critical Evaluation of the Current Parameterization, J. Geophys. Res. Atmos., 123(22), 12,994-13,015, doi:10.1029/2018JD029358, 2018.

McNamara, S. M., Kolesar, K. R., Wang, S., Kirpes, R. M., May, N. W., Gunsch, M. J., Cook, R. D., Fuentes, J. D., Hornbrook, R. S., Apel, E. C., China, S., Laskin, A. and Pratt, K. A.: Observation of Road Salt Aerosol Driving Inland Wintertime Atmospheric Chlorine Chemistry, ACS Cent. Sci., 5, doi:10.1021/acscentsci.9b00994, 2020.

McNamara, S. M., Chen, Q., Edebeli, J., Kulju, K. D., Mumpfield, J., Fuentes, J. D., Bertman, S. B. and Pratt, K. A.: Observation of N2O5 deposition and ClNO2 production on the saline snowpack, ACS Earth Sp. Chem., doi:10.1021/acsearthspacechem.0c00317, 2021.

Royer, H. M., Mitroo, D., Hayes, S. M., Haas, S. M., Pratt, K. A., Blackwelder, P. L., Gill, T. E. and Gaston, C. J.: The role of hydrates, competing chemical constituents, and surface composition on ClNO2formation, Environ. Sci. Technol., 55(5), 2869–2877, doi:10.1021/acs.est.0c06067, 2021.

Saunders, S. M., Jenkin, M. E., Derwent, R. G. and Pilling, M. J.: Protocol for the development of the Master Chemical Mechanism, MCM v3 (Part A): Tropospheric degradation of non-aromatic volatile organic compounds, Atmos. Chem. Phys., 3(1), 161–180, doi:10.5194/acp-3-161-2003, 2003.

Wang, S., McNamara, S. M., Kolesar, K. R., May, N. W., Fuentes, J. D., Cook, R. D., Gunsch, M. J., Mattson, C. N., Hornbrook, R. S., Apel, E. C. and Pratt, K. A.: Urban Snowpack ClNO2Production and Fate: A One-Dimensional Modeling Study, ACS Earth Sp. Chem., 4(7), 1140–1148, doi:10.1021/acsearthspacechem.0c00116, 2020.